Consolidation of clay slurry under very low stresses: from novel oedometer apparatus invention to non-linear consolidation characteristics and finite strain modelling

Peng-Lin LI, Postdoc Fellow

Department of Civil and Environmental Engineering, The Hong Kong Polytechnic University, Hung Hom, Kowloon, Hong Kong, China; email: pengl.li@connect.polyu.hk

Zhen-Yu YIN, Professor (corresponding author)

Department of Civil and Environmental Engineering, The Hong Kong Polytechnic University, Hung Hom, Kowloon, Hong Kong, China; Research Centre for Resources Engineering towards Carbon Neutrality (RCRE), The Hong Kong Polytechnic University, Hung Hom, Kowloon, Hong Kong, China; email: zhenyu.yin@polyu.edu.hk

Ding-Bao SONG, Research Assistant Professor

Department of Civil and Environmental Engineering, The Hong Kong Polytechnic University, Hung Hom, Kowloon, Hong Kong, China; email: dingbao.song@polyu.edu.hk; Dingbao_song@126.com

Ze-Jian CHEN, Research Assistant Professor

Department of Civil and Environmental Engineering, The Hong Kong Polytechnic University, Hung Hom, Kowloon, Hong Kong, China; email: zejian.chen@polyu.edu.hk;

Jian-Hua YIN, Chair Professor

Department of Civil and Environmental Engineering, The Hong Kong Polytechnic University, Hung Hom, Kowloon, Hong Kong, China; email: jian-hua.yin@polyu.edu.hk

Accepted version submitted to *Canadian Geotechnical Journal*

April 6, 2025

Abstract: This study first invents a novel oedometer apparatus for clay slurry, featuring a lightweight acrylic loading cap, a non-contact laser displacement sensor, and a 1:1 dead-weight loading system to improve traditional consolidation devices. The novel apparatus is then used to examine two clays: Hong Kong Marine Deposit and Kaolin clay. The loading with a minimum stress of 0.025 kPa is applied on samples with a maximum initial water content exceeding 9 times the liquid limit. Results demonstrate the "S" shape compression curves influenced by initial water contents, and the power-type relationships between permeability coefficient and void ratio. Empirical equations are obtained to determine the yield stress point based on initial water content and liquid limit. Higher initial water contents increase compression parameters (e.g., recompression index, C_r; compression index, C_c; and creep index, C_α), though C_r/C_c and C_α/C_c are almost in the normal range. The C_c of Kaolin clay with initial water contents above 3.5 times the liquid limit is significantly relevant to effective stress. Finally, a non-linear creep model is enhanced and integrated into the finite strain consolidation equations, effectively simulating the oedometer tests and a self-weight consolidation test of clay slurry with non-linear consolidation characteristics.

Keywords: clay; high initial water contents; consolidation; oedometer test; creep; constitutive model

1 Introduction

Many countries have used or prepared to reuse dredged deposits as fill materials in reclamation projects (Chu et al., 2006) to solve the short supply problem of land. The initial state of the dredged deposits used in reclamation is usually a slurry state with very high initial water contents typically higher than 100%, even ranging from 300% to 800% (Xu et al., 2012; Song et al., 2022). The finite strain consolidation will then occur under the self-weight and/or other loads (e.g., surcharge and vacuum loading). To accurately predict the consolidation process, it is necessary to explore the consolidation behaviour of clay with high initial water contents.

Current experimental methodologies to investigate the consolidation behaviour of clay with high initial water contents are primarily categorized into three distinct groups. One such approach involves the self-wight consolidation model test, also known as settling column test. Imai (1980) and Been and Sills (1981) conducted relevant experiments earlier. Been and Sills (1981) set a series of laboratory cylinder settling column model tests on clays with high initial water contents, measuring density by a non-destructive X-ray technique, total stress, pore pressure, and surface settlement. Density measurements facilitated the determination of void ratios, while effective stress was calculated from the difference between total stress and excess pore water pressure. This method enabled the derivation of compression curves for clay with high initial water contents. Bartholomeeusen et al. (2002), Alexis et al. (2004), and Bonin et al. (2014) provided a detailed analysis of the self-weight consolidation process of thick tailing layers for obtaining the compressibility relationship under low vertical effective stresses. A notable limitation of this method for obtaining compression curves is the difficulty in accurately measuring density and pore water pressure, particularly under low-stress ranges (Toorman, 1999). Li et al. (2013) proposed a straightforward method for measuring compression and permeability parameters based on data from column tests. Stress is still not easily controlled in the self-wight consolidation test. Another limitation of this kind of test is the requirement for taller columns to induce higher effective stresses. In addition, a seepage-induced consolidation testing system has been proposed and applied to explore the consolidation characteristics of clays with high initial water contents. Imai (1979) initially proposed this novel consolidation test method using seepage force, which was later modified by Fox and Baxter (1997). Berilgen et al. (2006) carried out some seepage-induced consolidation tests starting from very low-pressure levels (e.g., 0.25-2.00 kPa). The seepage-induced consolidation testing system is divided into two stages: initial consolidation facilitated by seepage followed by compression through loading. This method is not simple enough for wide application due to the difficulty in measuring the local pore pressure and the potential formation of preferential flow.

To enhance the applicability and controllability of small stress consolidation tests, several modifications were made to the traditional oedometer apparatus. A major challenge in conducting consolidation tests on clay with high initial water contents using a standard oedometer apparatus is preventing the clay from extruding from the cell due to the relatively large dead weight. To solve this problem, Hong et al. (2010) modified the typical oedometer test apparatus, adopting a 1:1 loading system and replacing the metal cap with a lighter loading cap. The 1:1 loading system was designed to apply the stress below 12.5 kPa. The function of the slight loading cap is to ensure that the applied small stress does not cause the clay with high initial water contents to extrude from the cell. Tests initiating at a stress of 0.5 kPa were conducted on clays with initial water contents ranging from 0.7 to 2.0 times their liquid limits. Zeng et al. (2015) and Zeng et al. (2016) investigated one-dimensional (1D) consolidation features of various natural clays and Kaolin clay with different initial water contents, utilizing the modified apparatus designed by Hong et al. (2010). One limitation of this apparatus is that the consolidation features of clay with high initial water contents under stress smaller than 0.5 kPa were not easily realized. This limitation arises because the minimum vertical stress, induced by the weight of the cap, the porous stone, and the elastic force of the dial gauge measuring rod cannot be completely alleviated. Even with a lightweight acrylic cap and a thin, porous stone (e.g., 5 mm thickness), a stress of approximately 0.5 kPa is generated, sufficient to extrude the clay with high initial water contents from the cell. Xu et al. (2015) performed oedometer tests on three distinct types of dredged clays, each with a maximum initial water content of approximately 4 times the liquid limit, using an enhanced apparatus. This apparatus balanced the weight of the cap and the porous stone before adding dead weight, thereby extending the minimum vertical stress to 0.1 kPa using a fixed pulley system. The maximum vertical stress of 15 kPa can be added to the clay with high initial water contents due to the infeasibility of connecting the apparatus to a leverage loading system. Similar to Xu et al. (2015), a self-made consolidation apparatus by Song et al. (2023) was also applied to explore the consolidation behaviour of clay with high initial water contents. The issue of elastic stress caused by the measuring rod in displacement measurement devices such as dial gauges or LVDTs remains unresolved. Consequently, this condition leads to a fixed pressure being automatically applied to the soil sample. Chai et al. (2019) also designed an oedometer device with a 1:1 loading system and carried out a series of tests starting from 0.5 kPa vertical stress. The aforementioned research predominantly focuses on clays with initial water contents less than 3-4 times the liquid limit. It is necessary to conduct a series of tests on clay with higher initial water contents to enhance the understanding of its consolidation behaviour. The test methods summarized above are predominantly utilized to investigate the 1D consolidation behavior of very soft soils and to derive their corresponding consolidation parameters. Notably, aside from the aforementioned experimental methods, back-analysis techniques have demonstrated efficacy in determining consolidation parameters such as compressibility and permeability parameters, as comprehensively reviewed by Vasudev and Bharat (2025). Taking some typical studies as examples, Bharat and Sharma (2011) proposed a back-analysis method employing natural computation algorithms to derive both compression parameters and hydraulic conductivity from the settlement curves of soft soils. Qi and Simms (2020) advanced more robust methodologies for accurately estimating soil consolidation parameters. Qi et al. (2020) further considered the synchronous occurrence of sedimentation and consolidation in predicting hydraulic conductivity. Building upon the 1D large strain consolidation framework established in centrifuge environments by Bharat and Ubaid (2019), Vasudev and Bharat (2022) introduced an innovative methodology for predicting the hydraulic conductivity of slurries from centrifuge consolidation settlements. Vasudev and Bharat (2022, 2025) further incorporated advanced optimization algorithms to enhance the precision of back-calculating hydraulic conductivity function parameters.

Further, the consolidation behaviour of clay with high initial water contents under small stress is significant for finite strain consolidation calculation. Many consolidation models were proposed in the past decades for describing the material nonlinearity and geometric nonlinearity of clay with high initial water contents (Gibson et al., 1967, 1981; Monte and Krizek, 1976; Toorman, 1999; Li et al., 2023; Song et al., 2023; Sun et al., 2023). The material nonlinearity mainly means that the compression parameters and permeability coefficients are related to the stress or void ratio state. Existing 1D compression models used in finite strain consolidation modelling mostly assumed that the relationship of vertical effective stress σ_z' and void ratio e is linear in $e-\log_{10}\sigma_z'$ coordinate system. In other words, the compression index C_c defined as the slope of the normal compression line (NCL) was assumed a constant in finite strain consolidation analysis. However, much experimental evidence indicates that the compression curves of many clays with high initial water contents exhibit obvious non-linear features in $e-\log_{10}\sigma_z'$ coordinate system especially in the small stress range (Girault, 1960; Bjerrum, 1967; Xu et al., 2015; Khan and Azam, 2016). The C_c changes with the void ratio or effective stress. In theory, a constant C_c value also causes the void ratios to become negative values if the effective stress is large enough. This problem is especially prominent in clay with high water content because its C_c is usually relatively large. Therefore, the compression constitution model with a compression limit is more suitable and necessary. Empirical power functions were proposed and extended to describe the non-linear feature of compression curves by Carrier (1983) and Liu and Znidarčić (1991). Butterfield (1979) and Hong et al. (2010) also proposed that the $\log_{10}(1+e)-\log_{10}\sigma_z'$ coordinate is more suitable for describing the compression behaviour of clay with high water contents. However, the $\log_{10}(1+e)-\log_{10}\sigma_z'$ coordinate is not suitable enough when the change range of C_c is very large. Furthermore, creep plays a significant role in the consolidation analysis, particularly for clayey soils. Several studies have addressed the influence of creep on large strain consolidation. For instance, Li et al. (2023) introduced an enhanced 1D Yin-Graham elastic viscoplastic (EVP) model suitable for slurry into the large strain consolidation model. Gheisari (2023) and Gheisari et al. (2023) incorporated several typical creep models into large strain consolidation analysis, providing a comparative discussion on the variations in the calculation results of each model. Song et al. (2023) further incorporated the creep limit into the piecewise large strain consolidation model reported by Fox and Baxter (1997). Shi et al. (2024) developed the 1D piecewise-linear large-strain consolidation model for soft clay with anisotropic creep behaviour. However, these studies did not address the varying nature of the compression index C_c.

This study investigates the consolidation behaviour of clay slurry with high initial water contents. A novel oedometer apparatus was developed by expanding the dimensions of the conventional oedometer cell and introducing a minor cap element to serve as a 1:1 load system. A fixed bully apparatus was employed to offset the combined weight of the cap and porous stone, thereby enabling incremental stress levels to the soil. The laser displacement sensor is applied to avoid the influence of the measuring rod of the dial gauge or LVDT. Oedometer tests were conducted using the new apparatus on two clays with a maximum water content of approximately nine times the liquid limit. The compressibility and permeability characteristics of clay with high water contents were analysed according to the test data. Finally, a non-linear compression model considering creep was proposed and verified using the test data. The non-linear model was further extended and integrated into the finite strain consolidation model and applied to a field test.

2 Experimental programs

2.1 Modified experimental apparatus

In this study, an enhanced oedometer apparatus, as present in Fig. 1, was developed, based on the conventional oedometer test apparatus. A fixed pulley system and a load-bearing tray were integrated to counterbalance the stress induced by the inherent gravitational forces of the cap and porous stone. The cap and porous stone have been interconnected to form a cohesive unit. The cap transitioned from metallic to plexiglass material. The conventional dial gauge or LVDT displacement measurement approach was replaced by a non-contact laser displacement sensor. This modification allows for the avoidance of elastic stress typically induced by the measurement rod in the dial gauge or LVDT. These enhancements to the traditional oedometer apparatus enable theoretical step-by-step loading from 0 kPa and prevent the extrusion of high-water-content clay from the cell. To facilitate the steady application of lower stresses, the diameter of the oedometer cell was increased to 140 mm, approximately twice that of the traditional oedometer cell. Slots of varying sizes have been symmetrically introduced on the plexiglass cap to facilitate 1:1 loading in the lower stress range. The modified oedometer was used in conjunction with the leverage system of a typical oedometer apparatus to apply large stresses. Additionally, an electronic scale was installed between the loading cap and fixed pulley to accurately quantify the weight applied to the soil. To ensure the evenness of the contact surface between the soil and the cap, multiple lightweight level bubbles have been strategically positioned on the plexiglass cap. As a result of these modifications, the compression curve now encompasses a significantly broader range of applied vertical stresses and initial water content conditions, as illustrated in Fig. 2. Specifically, the device can apply an expanded range of stresses, spanning from ultra-low stress levels (e.g., 0.025 kPa) to those commonly achievable with conventional oedometer devices. The device is also suitable for soils in various initial states, including clay slurries with very high initial water content (e.g., 7-8LL) and negligible strength unsuitable for traditional oedometer apparatuses, as well as low water content soil samples exhibiting an obvious strength.

2.2 Test material

Two different types of clays were selected to be used in the tests. One was the Hong Kong Marine Deposit (HKMD), primarily composed of silt and approximately 17% clay (particles with a diameter of less than 2 μm). The other material is a type of Kaolin clay, which comprises a significant 53% of the overall clay composition. Fig. 3 illustrates the particle size distribution of the two test soils. Table 1 lists the physical properties including liquid limits, plastic limits, and specific gravities of the test soils. The mineral compositions of the two test soils are detailed in Table 2. For HKMD, quartz represents the predominant mineral composition, accounting for 47.5%, while the Kaolin clay primarily consists of kaolinite, comprising 96.5%.

2.3 Test procedure

1D incremental loading consolidation tests were performed on HKMD and Kaolin clay with different initial water contents employing the improved oedometer apparatus. The initial conditions of the soil sample and planned loading schedules are listed in Table 3. The first vertical stress is 0.025 kPa and then gradually increases to 1 kPa by following the steps of 0.05 kPa, 0.1 kPa, 0.25 kPa, 0.5 kPa, and 1 kPa. The stress range 0.025-1 kPa was applied using the 1:1 loading system as shown in Fig. 1 (a). The vertical stresses of 2.5 kPa, 5 kPa, 10 kPa, 25 kPa, 50 kPa, and 100 kPa are subsequently applied by adding slotted weights on the 1:10 leverage loading system in a standard oedometer apparatus (Fig. 1 (b)). The loading time interval for each load level is 24 hours.

3 Results and Discussion

3.1 Relationships of void ratio versus effective stress

Fig. 4 illustrates the compression curves, depicting changes in void ratio e against effective stress σ' in a semi-logarithmic plot, of the two clays (i.e., HKMD and Kaolin clay). The initial water content significantly influences the compression features of the two test clays. The compression curves exhibit an inverse "S" shape which is consistent with the observation described by Hong et al. (2010). Xu et al. (2015) reported a phenomenon that the inverse "S" shape of compression curve vanishes, and the curve presents a concave upward shape when the initial water content is sufficiently high. This may occur because the compression behaviour with small stress under 0.1 kPa was not applied on the soil, resulting in the observation of the "S" shape. When test data under stress below 0.1 kPa are included (as shown in Fig. 3), the inverse "S" shape persists, even when the initial water content exceeds eight times the liquid limit. The inverse "S" shape also indicates the presence of a specific stress that decreases with increasing initial water contents. Compressibility increases once the vertical stress exceeds the remoulded yield stress. This phenomenon aligns well with the results presented by Hong et al. (2010). The specific stress is discussed in the subsequent section. Additionally, for both HKMD and Kaolin clay, the compression curves associated with higher initial water contents are positioned above that of clays with low initial water contents. This indicates that the initial water content significantly impacts the compression behaviour of clays. Interestingly, the compression curve of the Kaolin clay exhibits more pronounced non-linear characteristics than that of HKMD in $e-\log_{10}\sigma_z'$ coordinate system, especially when the initial water content increases to 8 times the liquid limit. This may be attributed to the markedly different mineral compositions of the two soils. The differing mineral compositions result in substantial structural differences between the two soils. The higher kaolinite content of Kaolin clay makes its structure mainly flocculation structure which is affected by initial water contents (Chai et al., 2019).

Additionally, various mechanisms, including large strain consolidation and sedimentation, can significantly influence slurry settlement behavior, potentially contributing to variations in the compression index C_c. A detailed analysis of this point is warranted to further understand the mechanisms involved. Previous studies have shown that the void ratio at the beginning of consolidation is approximately seven times the void ratio, e_L, at the liquid limit (Monte and Krizek, 1976; Carrier et al., 1983). Fig. 4 illustrates that all void ratios in the compression curves are lower than seven times the void ratio e_L at the liquid limit for HKMD and Kaolin clay. While the maximum initial void ratios (e.g., $9.2e_L$ for HKMD and $8.4e_L$ for Kaolin clay) slightly exceed seven times the void ratio at the liquid limit, they decrease to acceptable levels under a minimum applied stress of 0.025 kPa. Consequently, the compression curves shown in Fig. 4 are interpreted as interpreted as representing solely consolidation mechanisms, with sedimentation effects effectively excluded. Although the methodology adopted in this study to distinguish between consolidation and sedimentation mechanisms has inherent limitations, it offers a practical and feasible solution. Future efforts will prioritize comprehensive experimental investigations and advanced modeling techniques to isolate the contributions of individual mechanisms.

3.2 Relationships of void ratio versus permeability coefficient

The relationships between void ratio e and permeability coefficient k of HKMD and Kaolin clay with different initial water contents are shown in Fig. 5. The permeability coefficient k was determined following the Casagrande's method as detailed in Zeng et al. (2020a). As depicted in Fig. 5, there exists a strong correlation between the permeability coefficient and the void ratio for both HKMD and Kaolin clay, conforming approximately to a power function, e.g., $k=8.06\times10^{-6}e^{1.93}$ m/day (HKMD) and $k=3.21\times10^{-7}e^{3.35}$ (Kaolin clay). As the void ratio increases, the permeability coefficient also increases. The influence of initial water contents on the correlation between the permeability coefficient and the void ratio is not pronounced. These findings on the permeability coefficient of clay with high initial water contents are consistent with the results from Zeng et al. (2020b).

3.3 Relationships of initial water content versus remoulded yield stress

From Fig. 4, it is interesting to find that there a particular stress point in every stress-strain curve. When the effective stress is smaller than the stress of this point, the compressibility is low and then the compressibility increases with effective stress further increasing. The reason for causing the low compressibility in the range of low stresses smaller than the remoulded yield stress may be that grains stick together when mixed with water due to pore water suction and physicochemical pore fluid-mineral interaction Mitchell and Soga (2005). This cohesion is diminished as the water content increases, leading to a predominance of fluid in the soil-water mixture, which results in a decrease in remoulded yield stress. When the applied stress exceeds the remoulded yield stress, the cohesion between the soil and water because of the interaction is disrupted. This causes a dramatic increase in compressibility. The stress of this point was also reported by Mitchell and Soga (2005), Hong et al. (2010), and Hong et al. (2012). Mitchell and Soga (2005) first called this stress 'pore water suction'. Hong et al. (2010) and Hong et al. (2012) termed this stress as 'suction pressure' and 'remoulded yield stress'. In this study, the 'remoulded yield stress' was preferred for two reasons as the remoulded yield stress can distinguish with suction in unsaturated soil features and avoid confusion with the consolidation yield stress widely described in natural clay. Fig. 6 illustrates the method for determining this particular stress point. The compression curve with a constant C_c (Fig. 6 (a)) typically exhibits two linear segments in $e - \log_{10} \sigma'_z$ coordinate system. The point of intersection between these two segments is defined as the particular stress point. In the case of compression curves with noticeable variation in C_c, the sharply increasing compressibility part forms a distinct curve, which can be approximated as a series of linear segments, as shown in Fig. 6 (b). The point of intersection between the first linear segment within this series of segments and the low-stress linear segment is regarded as the particular stress point. Hong et al. (2010) and Hong et al. (2012) have proposed some relationships between the remoulded yield stress $\log_{10}\sigma'_{z,yr}$ and void ratio e_L at liquid limit, e.g., $\sigma'_{z,yr}=5.66/\left(e_0/e_L\right)^2$, where e_0 is initial void ratio. The relationship is applicable for the reconstituted clays with initial water contents of 0.7-2 times the liquid limit discussed by Hong et al. (2010). By further adding the fitting of the test data observed in this study which covered a wider range of initial water contents such as 2.7-8.4 times liquid limits, the optimum equation $\sigma'_{z,yr}=5.65/\left(e_0/e_L\right)^{2.01}$ in Fig. 7 is found which is almost the same as the equation of Hong et al. (2010). Similarly, as shown in Fig. 8, the ratio of void ratio at remoulded yield stress to void ratio at liquid limit can be expressed using the equation $e_{yr}/e_L=1.86/\left(\sigma'_{yr}\right)^{0.38}$ which is very close to the equation $e_{yr}/e_L=2/\left(\sigma'_{yr}\right)^{0.42}$ presented by Hong et al. (2010). According to these two equations, this particular state point can be determined using e_0 and e_L. This point is not only can help to further understand the deformation behaviour of reconstituted clays but also can applied to develop a compression model considering the influence of the initial void ratio on the compression behaviour. The compression model is significant in making the consolidation calculation of clay with high initial water contents more accurate.

3.4 Relationships of initial water content versus compression parameters

Fig. 9 and Fig. 10 show the compression parameters of HKMD and Kaolin clay with different initial water contents, including recompression index or swelling index $C_r=\Delta e/\Delta\log_{10}\left(\sigma'_z\right)$ for unloading-reloading, compression index C_c for normal compression, and creep index $C_\alpha=\Delta e/\Delta\log_{10}\left(t\right)$. It should be noted that C_c is assumed as constant in this section in order to discuss the influence of initial water contents on the average compressibility. As indicated by Fig. 9 and Fig. 10, the initial water content markedly influences the compression parameters. Typically, for normal clay, the compression index C_c ranges from 0.2 to 1.2 (Mitchell and Soga, 2005; Knappett and Craig, 2019; Zhang et al., 2021). Both HKMD and Kaolin clay, characterized by high initial water contents, have large compressibility, especially for Kaolin clay whose compression indexes are larger than the normal values. This phenomenon is consistent with the results reported by Xu et al. (2015). Similar patterns are evident for both the recompression index C_r and creep index C_α. When the initial water content exceeds two times the liquid limit, C_r and C_α fall within the higher range. However, the values of C_r/C_c and C_α/C_c were in the range of 0.1-0.3 and 0.01-0.03 which is close to the normal ranges, e.g., C_r/C_c=0.1-0.2 (Yin, 2013), and C_α/C_c=0.01-0.07 (Mesri and Castro, 1987; Wu et al., 2019). On the other hand, the indexes increase with the initial water contents for both HKMD and Kaolin clay. Therefore, the C_α/C_c is still a practical tool for calculating deformation due to creep in the consolidation process of clay with high water contents.

In Fig. 9 and Fig. 10, the compression indexes are obtained by fitting the effective stress-void ratio curve after the remoulded yield stress using the equation $e = e_0 - C_c \log_{10} \sigma'_z$. These values represent the average compressibility within the tested stress range. However, as evident from Fig. 4, the compression index C_c varies with effective stress for Kaolin clay, particularly when initial water contents exceed 3.5 times the liquid limit. To clarify the evolution of compressibility with changes in effective stress, Fig. 11 displays the compression indexes C_c of HKMD and Kaolin clay under various effective stresses. Fig. 11 indicates that the compression indexes are in a s narrower range of 1±0.25, compared to those for Kaolin clay. The C_c values of Kaolin clay decrease rapidly as effective stress increases. This phenomenon becomes more pronounced with higher initial water contents. By fitting the experimental data with various non-linear functions, the relationship between the compression index C_c and effective stress σ_z' was found to more closely resemble a power function. This finding offers valuable insights into selecting appropriate compression models to describe non-linear compression behaviour.

4 1D non-linear model and its application

4.1 Development of 1D non-linear compression model

According to results from the 1D consolidation test, a big difference between clay with high and low water contents (e.g., below liquid limit) is that the compressibility is significantly affected by the initial water content state and the compression curves are not linear in $e-\log_{10}\sigma_z'$ coordinate system for some cases. It is reasonable since a negative value of the void ratio will occur when the effective stress σ_z' is approaching infinite if the compression curves are linear in $e-\log_{10}\sigma_z'$ coordinate system. In other words, there exists a compression limit within the compression curve. This issue is particularly pronounced in clay with very high initial water contents, attributed to their high compression coefficients. The compression curves of the Kaolin clay with high water contents have apparent non-linear features in $e-\log_{10}\sigma_z'$ coordinate system, a finding also reported by previous studies (Girault, 1960; Bjerrum, 1967; Xu et al., 2015; Khan and Azam, 2016). Therefore, there is a need to develop a compression model to make up for the limitations of current widely used compression models which assume the compression curve is linear in $e-\log_{10}\sigma_z'$ coordinate system, e.g., for a normal consolidation soil the void ratio $e=e_{z0}-C_c\log_{10}\left(\sigma_z'/\sigma_{z0}'\right)$.

Fig. 11 characterizes the non-linear behaviour of void ratio-effective stress curves in $e-\log_{10}\sigma'_z$ coordinate system. To emphasize this characteristic, the hyperbolic function, successfully utilized by Kondner (1963) to define the stress-strain relationship and Yin (1999) to develop a creep model with a limit, was adopted. The hyperbolic function not only guarantees the existence of a limit value as effective stress approaches infinity but also shares similar non-linear features with the power function. Furthermore, to ensure that the compression model remains meaningful even when the effective stress is zero, it is suggested to adopt a compression relationship characterized by a defined compression limit, as follows:

$$e^r = e_0^r - \frac{C_{c0}\log_{10}\dfrac{\sigma'_z+\sigma'_{ref}}{\sigma'_{z0}+\sigma'_{ref}}}{1+\dfrac{C_{c0}}{e_0-e_l^r}\log_{10}\dfrac{\sigma'_z+\sigma'_{ref}}{\sigma'_{z0}+\sigma'_{ref}}} \tag{1}$$

where e_0^r is the void ratio at stress $\sigma'_z=\sigma'_{z0}$ in the normal consolidation line, e_l^r is the limit void ratio of the reference time line, the item $\left(e_0-e_l^r\right)$ has the meaning of maximum void ratio change value when $\sigma'_z \Rightarrow \infty$, σ'_{ref} is a reference stress for making sure the relation is still available when the effective stress is 0 or near 0, e.g., effective stress at the surface of the soil ground, e_0 is the initial void ratio, C_{c0} is a parameter related to the traditional compression index C_c, which can be expressed using:

$$C_c = \frac{C_{c0}}{1+\dfrac{C_{c0}}{\left(e_0-e_l^r\right)}\log_{10}\dfrac{\sigma'_z+\sigma'_{ref}}{\sigma'_{z0}+\sigma'_{ref}}} \tag{2}$$

In addition, the elastic section of the compression curve still uses the expression:

$$e = e_0^r - C_r\log_{10}\frac{\sigma'_{z0}+\sigma'_{ref}}{\sigma'_z+\sigma'_{ref}} \tag{3}$$

The point $\left(e_{yr},\sigma'_{z,yr}\right)$ can also be used instead of $\left(e_{z0},\sigma'_{z0}\right)$, then Equations (1) and (3) can be expressed as followed:

$$e = e_{yr} - \frac{C_{c0}\log_{10}\dfrac{\sigma'_z+\sigma'_{ref}}{\sigma'_{z,yr}+\sigma'_{ref}}}{1+\dfrac{C_{c0}}{\left(e_0-e_l^r\right)}\log_{10}\dfrac{\sigma'_z+\sigma'_{ref}}{\sigma'_{z,yr}+\sigma'_{ref}}} \tag{4}$$

$$e = e_{yr} - C_r\log_{10}\frac{\sigma'_{z,yr}+\sigma'_{ref}}{\sigma'_z+\sigma'_{ref}} \tag{5}$$

Further considering creep strain of soil by incorporating the 1D Yin-Graham EVP model (Yin and Graham, 1989, 1994), one can obtain:

$$e = e_0^r - \frac{C_{c0}}{1+\dfrac{C_{c0}}{e_0-e_l^r}\ln\dfrac{\sigma'_z+\sigma'_{ref}}{\sigma'_{z0}+\sigma'_{ref}}}\log_{10}\frac{\sigma'_z+\sigma'_{ref}}{\sigma'_{z0}+\sigma'_{ref}} - C_\alpha\log_{10}\left(\frac{t_0+t_e}{t_0}\right) \tag{6}$$

Or

$$e = e_{yr} - \frac{C_{c0}}{1+\dfrac{C_{c0}}{\left(e_0-e_l^r\right)}\log_{10}\dfrac{\sigma'_z+\sigma'_{ref}}{\sigma'_{z,yr}+\sigma'_{ref}}}\log_{10}\frac{\sigma'_z+\sigma'_{ref}}{\sigma'_{z,yr}+\sigma'_{ref}} - C_\alpha\log_{10}\left(\frac{t_0+t_e}{t_0}\right) \tag{7}$$

where t_e is the equivalent time, t_0 is reference time.

According to the proposed compression model illustrated in Fig. 12, the compression curves of clay with high initial water contents can be obtained by two distinct methods, as shown in Fig. 13. An optimal approach is to conduct oedometer tests using particular apparatus such as the enhanced apparatus in this study. Then the parameters in Equations (1) and (3) can be determined by fitting the test results. However, this method might not be sufficiently convenient due to the special equipment requirements. Therefore, a simplified and practical approach is proposed in this study. Firstly, point $\left(e_{yr},\sigma'_{z,yr}\right)$ can be calculated according to Equations

$\sigma'_{z,yr} = 5.65/\left(e_0/e_\mathrm{L}\right)^{2.01}$ and $e_{yr}/e_\mathrm{L} = 1.86/\left(\sigma'_{yr}\right)^{0.38}$, based on the initial water content and the liquid limit. Subsequently, the clays with high initial water contents are brought to a low water content state through simplified processing such as self-weight or pre-pressure. Standard oedometer tests are then conducted on the treated soils. Finally, Equations (4) and (5) are applied to fit the compression curve with point $\left(e_{yr}, \sigma'_{z,yr}\right)$. In this way, the influence of initial water contents on the compressibility can be considered.

4.2 Model verification

To verify the capability of capturing the non-linear compression features of clay with high initial water contents, oedometer test results exhibiting variable C_c values were collected to validate the reliability of the proposed models. The collected test data, along with results from this study, were utilized to fit Equations (4) and (5) or Equations (1) and (3). For comparison with traditional compression functions, the compression curves of Kaolin clay were employed to calibrate Equations (4) and (5). The fitting results are displayed in Fig. 14. The test data from Xu et al. (2015) served to verify the reliability of the non-linear compression model, as shown in Fig. 15. Owing to the absence of data before the remoulded yield stress, Equation (1) was used to fit the data reported by Xu et al. (2015). The fitting parameters are present in Table 4 and Table 5. The R^2 values of non-linear fitting are all larger than 0.99, which is better than the linear fitting with constant C_c. In cases of distinctly non-linear compression curves (e.g., Fig. 14), t employing a constant C_c to fit the test data results in a negative void ratio. Consequently, the non-linear compression model proves more suitable for describing the compression behaviour of clay with high initial water contents. It should be noted that Equation (1) remains capable of capturing the compression curve feature even as the curve approaches linearity in $e-\log_{10}\sigma_z'$ coordinate system as shown in Fig. 14 (d).

4.3 Extension to finite strain consolidation model

To further indicate the application prospect, the proposed non-linear compression model was incorporated into the 1D finite strain consolidation equations considering self-weight stress in Lagrangian coordinates (Li et al., 2023). The consolidation equations obey the vertical force equilibrium:

$$\frac{\partial\sigma_z}{\partial a}=\gamma_m=\frac{G_s+e}{1+e_0}\gamma_w \tag{8}$$

where σ_z is the total vertical stress, a is the vertical Lagrangian coordinate, γ_m the current unit weight of saturated soil, G_s the specific gravity of the soil particle and γ_w the unit weight of water.

Taking into the Darcian flow and the relative velocity of the fluid and solid phases in soil, one can obtain:

$$v=-ki \tag{9}$$

$$v=\frac{e}{1+e}\left(v_w-v_s\right) \tag{10}$$

$$\frac{e}{1+e}\left(v_w-v_s\right)=-\frac{k}{\gamma_w}\left(\frac{1+e_0}{1+e}\frac{\partial u_e}{\partial a}\right) \tag{11}$$

where v is the vertical velocity, k is permeability coefficient, which is a function of current void ratio e: $k=k(e)$, i is hydraulic gradient, v_w and v_s are vertical velocities of fluid and solid phases, u_e is the excess pore water pressure.

According to the continuity equation, the volume change of the soil element is equal to the difference between the water amount of flow into and out of the element in the unit time period, which can be expressed as follows:

$$\frac{\partial}{\partial a}\left[\frac{k}{\gamma_w}\left(\frac{1+e_0}{1+e}\frac{\partial u_e}{\partial a}\right)\right]=\frac{1}{1+e_0}\frac{\partial e}{\partial t} \tag{12}$$

where the expression of void ratio e can be expressed by Equations (4) and (5) or Equations (1) and (3).

In addition, according to the extended 1D EVP model on Equation (6), one can obtain:

$$t_0+t_e=10^{e^r_{z0}-e}t_0\left(\frac{\sigma'_z+\sigma'_{ref}}{\sigma'_{z0}+\sigma'_{ref}}\right)^{-\frac{C_{c0}}{1+\frac{C_{c0}}{e_0-e_l^r}\log_{10}\frac{\sigma'_z+\sigma'_{ref}}{\sigma'_{z0}+\sigma'_{ref}}}} \tag{13}$$

From Equation (13), ‘equivalent time’ t_e:

$$t_e=10^{e^r_{z0}-e}t_0\left(\frac{\sigma'_z+\sigma'_{ref}}{\sigma'_{z0}+\sigma'_{ref}}\right)^{-\frac{C_{c0}}{1+\frac{C_{c0}}{e_0-e_l^r}\log_{10}\frac{\sigma'_z+\sigma'_{ref}}{\sigma'_{z0}+\sigma'_{ref}}}}-t_0 \tag{14}$$

Differentiating Equation (6) with time, one can get:

$$\frac{\partial e^{vp}}{\partial t}=\frac{C_\alpha/\ln 10}{t_0+t_e} \tag{15}$$

Incorporating Equation (13), Equation (15) can be rewritten:

$$\frac{\partial e^{vp}}{\partial t}=\frac{C_\alpha/\ln 10}{10^{e^r_{z0}-e}t_0\left(\frac{\sigma'_z+\sigma'_{ref}}{\sigma'_{z0}+\sigma'_{ref}}\right)^{-\frac{C_{c0}}{1+\frac{C_{c0}}{e_0-e_l^r}\log_{10}\frac{\sigma'_z+\sigma'_{ref}}{\sigma'_{z0}+\sigma'_{ref}}}}} \tag{16}$$

Further, one can obtain:

$$\frac{\partial e}{\partial t}=\frac{C_r}{\ln 10}\frac{\partial \sigma'_z}{\partial t}\frac{1}{\sigma'_{ref}+\sigma'_z}+\frac{C_\alpha/\ln 10}{10^{e^r_{z0}-e}t_0\left(\frac{\sigma'_z+\sigma'_{ref}}{\sigma'_{z0}+\sigma'_{ref}}\right)^{-\frac{C_{c0}}{1+\frac{C_{c0}}{e_0-e_l^r}\log_{10}\frac{\sigma'_z+\sigma'_{ref}}{\sigma'_{z0}+\sigma'_{ref}}}}} \tag{17}$$

Incorporating the effective stress principle $\sigma_z' = \sigma_z - u_e$, Equation (17) could also be rewritten as:

$$\frac{\partial e}{\partial t} = \frac{C_r}{\ln 10}\frac{\partial\left(\sigma_z - u_e\right)}{\partial t}\frac{1}{\sigma_{ref}' + \left(\sigma_z - u_e\right)} + \frac{C_\alpha / \ln 10}{10^{e_{z0}^r - e} t_0 \left[\frac{\left(\sigma_z - u_e\right) + \sigma_{ref}'}{\sigma_{z0}' + \sigma_{ref}'}\right]^{-\frac{C_{c0}}{1+\frac{C_{c0}}{e_0 - e_l^r}\log_{10}\frac{(\sigma_z - u_e)+\sigma_{ref}'}{\sigma_{z0}'+\sigma_{ref}'}}}} \tag{18}$$

The finite strain consolidations Equations (12) and (18) are solved to obtain the void ratio and pore water pressure evolution using the coefficient-type partial differential equations (PDE) in the COMSOL PDE module.

4.4 Experimental verification

To demonstrate the reliability of the consolidation parameters obtained using the modified oedometer apparatus in this study, the test data for Kaolin clay, which exhibited large deformation and obviously non-linear compression, were simulated. Fig. 16 illustrates the evolution of both the simulated and measured void ratios of Kaolin clay with varying initial water contents. In the simulation, all consolidation parameters, encompassing the non-linear compression parameters (Table 4), creep parameters (Fig. 10(c)), and the permeability coefficient function (Fig. 5), were determined by the oedometer test tests conducted using the modified apparatus. A uniform permeability coefficient function and consistent compressibility curves were adopted across all stress levels. To be specific, Table 4 presents a detailed summary of the initial conditions and non-linear compression parameters applied in each scenario. Fig. 5 illustrates that the permeability coefficient functions of soil samples with varying initial water contents generally conform to the same relationship. Consequently, the simulations of the four tests, each with varying initial water contents, utilized an identical permeability coefficient function k=3.21×$10^{-7}e^{3.35}$ m/day. The creep parameters including t_0 and C_α are clearly marked on each deformation curve depicted in Fig. 16. The creep index shown in Fig. 16 exhibits variations across different stress levels. To provide a more intuitive representation of this characteristic, Fig. 17 illustrates the stress dependency of the creep index for Kaolin clay in this simulation. Fig. 17 illustrates that the creep index exhibits fluctuations in response to varying stress levels under different initial conditions. The overall trend reveals an initial increase, followed by a decline and eventual stabilization, aligning with some previous studies on creep deformation in clayey soils (Li et al., 2012; Zhu et al., 2014; Wu et al., 2019; Rezania et al., 2020). This phenomenon can be attributed to the dominant creep mechanisms at low stress levels, which involve viscous sliding between clay particles and the viscous flow of pore water. With increasing stress, the driving force intensifies, promoting particle rearrangement and pore water migration, which in turn leads to a gradual rise in the creep index. However, beyond a critical stress threshold, the interparticle structure compacts, and the clay fabric stabilizes at particle contacts, thereby reducing creep deformation at high stress levels and causing the creep index to decrease and stabilize.

The strong agreement between the calculated and monitored changes in the void ratio over time underscores the effective performance of the specially designed oedometer apparatus in providing the consolidation parameters of clay with very high water contents. The primary and secondary consolidation are both captured using the present consolidation model. The results also indicate the proposed non-linear compression model with creep is also effective for describing the compression features of clay with high initial water contents. In validating consolidation models, pore water pressure also plays a significant role. Pore water pressure and settlement data provide a comprehensive representation of the consolidation process in soils, offering valuable insights into whether the soil is undergoing primary or secondary consolidation. The pore water pressure measurements offer localized information on the consolidation state at specific positions. Settlement data reflect the overall deformation of the specimen across its entire height. Thus, utilizing both pore water pressure and settlement data as evaluation parameters significantly enhances the robustness of model validation. Furthermore, pore water pressure measurements, when combined with the applied total stress, allow for the derivation of the effective stress, which further ensures the accuracy of the obtained stress-strain relationship. This further underscores the indispensable role of pore water pressure data in consolidation model validation. In fact, we reserved threaded holes for the installation of pore water pressure sensors during the apparatus design and processing. However, due to the limitations in the accuracy of suitable pore water pressure sensors, the ultra-low stress levels involved in this study (e.g., 0.025 kPa) encountered in this study present significant challenges in achieving precise measurements. Consequently, similar to most conventional 1D consolidation tests, this study focused solely on monitoring settlement and comparing observed and simulated settlement data. The development and implementation of advanced technologies or high-precision pore water pressure sensors for measuring ultra-low pore water pressure, along with their integration into novel consolidation apparatus remains a key focus of ongoing research following this study.

4.5 Application to a field tank test

The oedometer test simulations were conducted on samples of relatively small dimensions, reflecting the limitations inherent to laboratory-scale studies. To enhance the reliability of model validation, a large-scale field tank test was employed to replicate the 1D finite strain consolidation behavior of slurry, with particular attention given to the variability in the compression index C_c. This approach offers valuable insights into the potential of the model for practical engineering applications. As reported by McVay (1986) and Fox and Berles (1997), the test involved a soil column with an initial height of 6.33 m, which began to consolidate under self-weight stress from a significantly high initial void ratio. More importantly, data from both laboratory and field tests, as shown in Fig. 18, reveal that the compression index changes as effective stress increases. The fitting effect of the present non-linear compression model with R^2=0.997 is much better than that of the constant compression model with R^2=0.569. R^2 is defined as the coefficient of determination, quantifying the accuracy of predictions in approximating actual data. The closer the R^2 value approaches 1, the better the prediction effect is. Given the absence of a creep parameter in the original study, the influence of creep on the consolidation process was intentionally omitted from the analysis. To demonstrate the importance of considering the highly non-linear compressibility and the performance of the proposed model, two simulations with a variable compression index and a constant compression index (as shown in Fig. 18) were conducted.

First, the non-linear compression model and permeability model were applied to fit the test data as shown in Fig. 18. The fitting parameters are shown in Table 6. Fig. 18 (a) illustrates that the proposed model, which considers non-linear compressibility, more accurately captures the compression data compared to the model with a constant compression index C_c. Furthermore, the calculated settlement and void ratio distributions, shown in Fig. 19, also highlight the importance of considering non-linear compression features in the $e-\log_{10}\sigma'_z$ coordinate system. Neglecting to consider non-linear compression led to an underestimation of the soil surface settlement. The predicted void ratios, when non-linear compression is not considered, exceed those observed in the test data.

5 Conclusions

This study introduced an enhanced oedometer test apparatus designed to investigate the consolidation behaviour of clay with high water contents. The improved apparatus was employed to perform oedometer tests on two clays, HKMD and Kaolin clay. A 1D non-linear compression model with a limit was proposed then and validated according to the experimental results. The potential applications of the present compression model were further demonstrated through its successful integration into finite strain consolidation analyses. According to the analysis, the following conclusions can be drawn:

(a) An enhanced oedometer apparatus was developed and utilized to investigate the consolidation behaviour of two clays with high initial water contents. The pulley apparatus, equipped with a weight tray, effectively offsets the weight of the cap and porous stone. The laser displacement sensor eliminated the stress typically induced by the measuring rod of the dial gauge or LVDT. Through the aforementioned enhancements to the conventional oedometer test apparatus, a minimal stress of 0.025 kPa was successfully applied to clays with high initial water contents exceeding 9 times the liquid limit.

(b) The initial water content significantly influences the shape of compression curves and compression-related indexes. However, the permeability coefficient is not very sensitive to the initial water contents. The average compressibility indexes, including C_r, C_c, and C_α tend to rise with an increase in initial water contents. However, the impact of initial water content on the ratios C_r/C_c and C_α/C_c values is not clearly evident. For Kaolin clay with an initial water content exceeding 3.5 times the liquid limit, the relationship between the compression index C_c and the effective stress σ'_z is negatively correlated. In addition, the relationships between the permeability coefficient and the void ratio are non-linear and can be described by a power function.

(c) The remoulded yield stress and its corresponding void ratio are related to the ratio of initial void ratio and void ratio at liquid limit. The equations $\sigma'_{z,yr} = 5.65/\left(e_0/e_\mathrm{L}\right)^{2.01}$ and $e_{yr}/e_\mathrm{L} = 1.86/\left(\sigma'_{yr}\right)^{0.38}$ can be adopted to obtain this particular state point. These equations have been verified as applicable to reconstituted clays with a wide range of initial water contents, ranging from 0.7 to 9.2 times their liquid limits.

(d) The proposed non-linear compression model, which incorporates a limit, is better suited for describing the compression curves of clay with high initial water contents characterized by apparent non-linear features in $e-\log_{10}\sigma'_z$ coordinate system. On one hand, the fit of test data using the non-linear compression model outperforms that of the linear compression model with a constant compression index C_c. On the other hand, the non-linear compression relationships

Equation (1) or Equation (5) address the limitations of the traditional logarithmic function, which may cause a negative void ratio and become meaningless as effective stress approaches zero. Two methods to determine the compression models of clay with high initial water contents are also proposed.

(e) Additionally, the proposed non-linear compression model has been extended to consider creep and integrated into the finite strain consolidation model. The finite strain consolidation model successfully simulated the oedometer tests and a self-weight consolidation test on clay with high initial water contents with non-linear compression characteristics. This confirmed the efficacy of the proposed non-linear compression model and its corresponding finite strain consolidation model.

Acknowledgments

The work in this paper is supported by a Research Impact Fund (RIF) project (R5037-18), a Theme-based Research Scheme Fund (TRS) project (T22-502/18-R), and three General Research Fund (GRF) projects (PolyU 152179/18E; PolyU 152130/19E; PolyU 152100/20E) from Research Grants Council (RGC) of Hong Kong Special Administrative Region Government of China. The authors also acknowledge the financial supports from Research Institute for Sustainable Urban Development of The Hong Kong Polytechnic University and a grant ZDBS from The Hong Kong Polytechnic University.

Data Availability Statement

All data that support the findings of this study are available from the corresponding author upon reasonable request.

References

Alexis, A., Lebras, G., and Thomas, P. 2004. Experimental bench for study of settling-consolidation soil formation. Geotechnical Testing Journal, **27**(6): 557-567.

Bartholomeeusen, G., Sills, G., Znidarčić, D., Van Kesteren, W., Merckelbach, L. M., Pyke, R., Carrier, W. D., Lin, H., Penumadu, D., Winterwerp, H.S., Masala, and Chan, D. 2002. Sidere: numerical prediction of large-strain consolidation. Géotechnique, **52**(9): 639-648.

Been, K., and G. C. Sills. 1981. Self-weight consolidation of soft soils: an experimental and theoretical study. Géotechnique, **31**(4): 519-535.

Berilgen, S., M. Berilgen, I. Ozaydin. 2006. Compression and permeability relationships in high water content clays. Applied Clay Science, **31**(3): 249-261.

Bharat, T. V., and Sharma, J. 2011. Prediction of compression and permeability characteristics of mine tailings using natural computation and large-strain consolidation framework. In Geo-Frontiers 2011: Advances in Geotechnical Engineering (pp. 3868-3877).

Bharat, T. V., and Ubaid, M. 2019. Analytical model for consolidation settlements under centrifuge environment. Canadian Geotechnical Journal, **56**(4): 484-494.

Bjerrum, L. 1967. Engineering geology of Norwegian normally-consolidated marine clays as related to settlements of buildings. Géotechnique, **17**(2): 83-118.

Bonin M. D., Nuth, M., Dagenais, A. M., and Cabral, A. R. 2014. Experimental study and numerical reproduction of self-weight consolidation behaviour of thickened tailings. Journal of Geotechnical and Geoenvironmental Engineering, **140**(12): 04014068.

Butterfield, R. 1979. A natural compression law for soils (an advance on *e*-logp'). Géotechnique, **29**(4): 469-480.

Carrier III, W. D., Bromwell, L. G., and Somogyi, F. 1983. Design capacity of slurried mineral waste ponds. Journal of Geotechnical Engineering, **109**(5): 699-716.

Carrier, W. D., Bromwell, L. G., and Somogyi, F. 1983. Design capacity of slurried mineral waste ponds. Journal of Geotechnical Engineering, **109**(5): 699-716.

Chai, J. C., Shen, S. L., and Geng, X. Y. 2019. Effect of initial water content and pore water chemistry on intrinsic compression behaviour. Marine Georesources & Geotechnology, **37**(4): 417-423.

Chu, J., Bo, M. W., and Choa., V. 2006. Improvement of ultra-soft soil using prefabricated vertical drains. Geotextiles and Geomembranes, **24**(6): 339-348.

Fox, P. J., and Baxter, C. D. 1997. Consolidation properties of soil slurries from hydraulic consolidation test. Journal of Geotechnical and Geoenvironmental Engineering, **123**(8): 770-776.

Fox, P. J., and Berles, J. D. 1997. CS2: a piecewise-linear model for large strain consolidation. International Journal for Numerical and Analytical Methods in Geomechanics, **21**(7): 453-475.

Gheisari, N. 2023. Large-strain consolidation analysis accounting for time-dependent effects in clayey tailings and soft soils (Doctoral dissertation, Carleton University).

Gheisari, N., Qi, S., and Simms, P. 2023. Incorporation of three different creep models into large-strain consolidation analysis of a clayey tailings deposit. Computers and Geotechnics, **161**: 105533.

Gibson, R. E., G. L. England, and M. J. L. Hussey. 1967. The theory of one-dimensional consolidation of saturated clays: I. finite non-linear consolidation of thin homogeneous layers. Géotechnique, **17**(3): 261-273.

Gibson, R. E., R. L. Schiffman, and K. W. Cargill. 1981. The theory of one-dimensional consolidation of saturated clays. II. Finite nonlinear consolidation of thick homogeneous layers. Canadian Geotechnical Journal, **18**(2): 280-293.

Girault, P. 1960. A study on the consolidation of Mexico City clay. PhD thesis, Purdue University, Lafayette, Indiana.

Hong, Z. S., J. Yin, and Y. J. Cui. 2010. Compression behaviour of reconstituted soils at high initial water contents. Géotechnique, **60**(9): 691-700.

Hong, Z. S., Zeng, L. L., Cui, Y. J., Cai, Y. Q., and Lin, C. 2012. Compression behaviour of natural and reconstituted clays. Géotechnique, **62**(4): 291-301.

Hong, Z., and Han, J. 2007. Evaluation of sample quality of sensitive clay using intrinsic compression concept. Journal of Geotechnical and Geoenvironmental Engineering, **133**(1): 83-90.

Imai, G. 1979. Development of a new consolidation test procedure using seepage force. Soils and Foundations, **19**(3): 45-60.

Imai, G. 1980. Settling behaviour of clay suspension. Soils and Foundations, **19**(2): 61-77.

Khan, F. S., and Azam, S. 2016. Determination of consolidation behaviour of clay slurries. International Journal of Mining Science and Technology, **26**(2): 277-283.

Knappett, J., and Craig, R. F. 2019. Craig's soil mechanics. CRC press.

Kondner, R. L. 1963. Hyperbolic stress-strain response: cohesive soils. Journal of the Soil Mechanics and Foundations Division, **89**(1): 115-143.

Li, L., Alvarez, I. C., and Aubertin, J. D. 2013. Self-weight consolidation of slurried deposition: tests and interpretation. International Journal of Geotechnical Engineering, **7**(2): 205-213.

Li, P. L., Yin, J. H., Yin, Z. Y., and Chen, Z. J. 2023. One-dimensional nonlinear finite strain analysis of self-weight consolidation of soft clay considering creep. Computers and Geotechnics, **153**: 105081.

Li, Q., Ng, C. W. W., and Liu, G. B. 2012. Low secondary compressibility and shear strength of Shanghai Clay. Journal of Central South University, **19**(8): 2323-2332.

Liu, J. C., and Znidarčić D. 1991. Modelling one-dimensional compression characteristics of soils. Journal of Geotechnical Engineering, **117**(1): 162-169.

McVay, M., Townsend, F., and Bloomquist, D. 1986. Quiescent consolidation of phosphatic waste clays. Journal of Geotechnical Engineering, **112**(11): 1033-1049.

Mesri, G., and Castro, A. 1987. C_a/C_c concept and K_0 during secondary compression. Journal of Geotechnical Engineering, **113**(3): 230-247.

Mitchell, J. K., and Soga, K. 2005. Fundamentals of soil behaviour (Vol. 3, p. USA). New York: John Wiley & Sons.

Monte, J. L., and Krizek, R. J. 1976. One-dimensional mathematical model for large-strain consolidation. Géotechnique, **26**(3): 495-510.

Qi, S., and Simms, P. 2020. Robust methods to estimate large-strain consolidation parameters from column experiments. Canadian Geotechnical Journal, 57(5), 683-705.

Qi, S., Chen, X., Simms, P., Zhou, J., and Yang, X. 2020. New method for determining the permeability function parameters of soft soils considering synchronous sedimentation and consolidation. Computers and Geotechnics, **127**: 103781.

Rezania, M., Bagheri, M., and Mousavi Nezhad, M. 2020. Creep and consolidation of a stiff clay under saturated and unsaturated conditions. Canadian Geotechnical Journal, **57**(5): 728-741.

Shi, J., Cao, Y., and Ling, D. 2024. One-dimensional piecewise-linear large-strain consolidation model for soft clay with anisotropic creep behaviour. European Journal of Environmental and Civil Engineering, **28**(7): 1565-1588.

Song, D. B., Lou, K., Yin, J. H., Fox, P. J., and Chen, W. B. 2023. A finite strain elastic-viscoplastic consolidation model for layered soft soils considering self-weight and nonlinear creep. Journal of Geotechnical and Geoenvironmental Engineering, **149**(12): 04023121.

Song, D. B., Pu, H. F., Khoteja, D., Li, Z. Y., and Yang, P. 2022. One-dimensional large-strain model for soft soil consolidation induced by vacuum-assisted prefabricated horizontal drain. European Journal of Environmental and Civil Engineering, **26**(11): 5496-5516.

Song, D. B., Pu, H. F., Yin, Z.-Y., Min, M., and Qiu., J. W. 2023. Plane-strain model for large strain consolidation induced by vacuum-assisted prefabricated horizontal drains. Int. J. Numer. Anal. Methods Geomech. 47(10), 1911-1935.

Song, M. M., Ding, J. W., Xiao, Q., Yin, J., and Xu, G. Z. 2023. Primary and secondary compression behaviour of dredged clay at low effective stresses. Marine Georesources & Geotechnology, **41**(2): 123-131.

Sun H. L., Zhang, H., Geng, X. Y., Cui Y. J., and Cai, Y. Q. 2023. Large-strain consolidation analysis for clayey sludge improved by horizontal drains. Journal of Geotechnical and Geoenvironmental Engineering, **149**(8): 04023057.

Tang, A. M., Cui, Y. J., Eslami, J., and Défossez, P. 2009. Analysing the form of the confined uniaxial compression curve of various soils. Geoderma. **148**(3-4): 282-290.

Toorman, E. A. 1999. Sedimentation and self-weight consolidation: constitutive equations and numerical modelling. Géotechnique, **49**(6): 709-726.

Vasudev, A., and Bharat, T. V. 2022. Prediction of hydraulic conductivity parameters of slurries from centrifuge consolidation settlements. Canadian Geotechnical Journal, **59**(11): 1981-2001.

Vasudev, A., and Bharat, T. V. 2022. Prediction of hydraulic conductivity function parameters of slurries using hybrid metaheuristics approach. In Indian Geotechnical Conference (pp. 15-27). Singapore: Springer Nature Singapore.

Vasudev, A., and Bharat, T. V. 2025. Prediction of permeability characteristics of mine slurries and sediments using finite-strain framework by optimisation algorithms. Expert Systems with Applications, 261, 125495.

Wu, Z. L., Deng, Y. F., Cui, Y. J., Zhou, A. N., Feng, Q., and Xue, H. C. 2019. Experimental study on creep behaviour in oedometer tests of reconstituted soft clays. International Journal of Geomechanics, **19**(3): 04018198.

Xu, G. Z., and Yin, J. 2016. Compression behaviour of secondary clay minerals at high initial water contents. Marine Georesources & Geotechnology, **34**(8): 721-728.

Xu, G. Z., Gao, Y. F., Hong, Z. S., and Ding, J. W. 2012. Sedimentation behaviour of four dredged slurries in China. Marine Georesources & Geotechnology, **30**(2): 143-156.

Xu, G. Z., Gao, Y. F., Yin, J., Yang, R., and Ni, J. 2015. Compression behaviour of dredged slurries at high water contents. Marine Georesources & Geotechnology, **33**(2): 99-108.

Yin, J. H. 1999. Non-linear creep of soils in oedometer tests. Géotechnique, **49**(5), 699-707.

Yin, J. H. 2011. From constitutive modelling to development of laboratory testing and optical fiber sensor monitoring technologies. Chinese Journal of Geotechnical Engineering, **33**(1): 1-15.

Yin, J. H. 2013. Review of elastic visco-plastic modelling of the time-dependent stress-strain behaviour of soils and its extensions and applications. Constitutive Modelling of Geomaterials: Advances and New Applications, Springer, Berlin, 149-157.

Yin, J. H., and G. Zhu. 2020. Consolidation analyses of soils. Boca Raton, FL, CRC Press.

Yin, J. H., and Graham, J. 1989. Visco-elastic-plastic modelling of one-dimensional time-dependent behaviour of clays. Canadian Geotechnical Journal, **26**(3): 199-209.

Yin, J. H., and Graham, J. 1994. Equivalent times and one-dimensional elastic viscoplastic modelling of time-dependent stress-strain behaviour of clays. Canadian Geotechnical Journal, **31**(1): 42-52.

Zeng, L. L., Cai, Y. Q., Cui, Y. J., and Hong, Z. S. 2020b. Hydraulic conductivity of reconstituted clays based on intrinsic compression. Géotechnique, 70(3): 268-275.

Zeng, L. L., Hong, Z. S., and Cui, Y. J. 2015. Determining the virgin compression lines of reconstituted clays at different initial water contents. Canadian Geotechnical Journal, **52**(9): 1408-1415.

Zeng, L. L., Hong, Z. S., and Cui, Y. J. 2016. Time-dependent compression behaviour of dredged clays at high water contents in China. Applied Clay Science, **123**: 320-328.

Zeng, L. L., Wang, H., and Hong, Z. S. 2020a. Hydraulic conductivity of naturally sedimented and reconstituted clays interpreted from consolidation tests. Engineering Geology, **272**: 105638.

Zhang, P., Yin, Z. Y., Jin, Y. F., Chan, T. H., and Gao, F. P. 2021. Intelligent modelling of clay compressibility using hybrid meta-heuristic and machine learning algorithms. Geoscience Frontiers, **12**(1): 441-452.

Zhu, Q., Yin, Z., Wu, Z., and Hicher, P. 2014. Uniqueness of time-dependencies for Shanghai soft clay. In Proc. 8th European Conf. on numerical methods in geotechnical engineering, Delft (pp. 139-143).

Tables

Table 1 Basic physical properties of test soils

Properties	HKMD	Kaolin clay
Specific gravity, G_s	2.62	2.58
Liquid limit, LL (%)	49	58
Plastic limit, PL (%)	31	33
Plastic index, PI (%)	18	25

Table 2 Mineral compositions of test soils

Items	HKMD	Kaolin clay
Quartz (%)	47.5	0.6
Kaolinite (%)	8.3	96.5
Illite (%)	-	2.9
Muscovite (%)	14.3	-
Clinochlore (%)	11.0	-
Microcline (%)	9.9	-
Albite (%)	5.8	-
Pyrite (%)	1.9	-
Calcite (%)	1.3	-

Table 3 Initial conditions and loading schedule of test soils

Soils	Initial water content (%)	Initial water content/LL
HKMD	131.2	2.7
	197.7	4.0
	312.7	6.4
	452.2	9.2
Kaolin clay	205.3	3.5
	258.8	4.5
	305.2	5.3
	487.0	8.4
Loading (kPa)	0.025→0.05→0.1→0.25→0.5→1→2.5→5→10→25 →50→25→10→5→10→25→50→100	

Table 4 Parameters in Equations (4) and (5) by best curve-fitting test data of Kaolin clay

Parameter	Kaolin clay			
	205.3%	258.8%	305.2%	487.0%
e_0	5.297	6.677	7.874	12.565
C_{c0}	5.692	6.283	6.312	8.337
e_l^r	0.00012	0.00015	0.00012	0.00025
C_r	0.231	0.250	0.271	0.283
σ'_{ref}	2.324	1.397	0.621	0.215

Table 5 Parameters in Equations (1) and (3) by best curve-fitting test data measured from Xu et al. (2015)

Parameter	Wenzhou slurry	Huaian slurry I	Huaian slurry II
	257.8%	171.6%	127.8%
e_0	6.986	4.633	3.387
e_{z0}	5.766	3.548	2.335
σ'_{z0}	0.174	0.159	0.191
C_{c0}	4.8647	2.368	1.112
e_l^r	0.00022	0.00027	0.0003
σ'_{ref}	0.1336	0.233	0.022

Table 6 Soil parameters in two self-weight consolidation simulations

Items	Changing compression index C_c	Constant compression index C_c
C_{c0} or C_c	7.13	6.45
C_α	-	-
e_0	18.8	18.8
σ'_{z0} (kPa)	0.224	0.224
e_l^r	0.001	-
k (m/s)	$2.016\times10^{-11}e^{4.048}$	$1.667\times10^{-11}(1+e)^{4.146}$

List of figure captions

Fig. 13 Methods to obtain the 1D compression relationship of clay with high initial water contents: (a) using enhanced oedometer apparatus; (b) using conventional oedometer apparatus

Fig. 14 Fitting compression curves of Kaolin clay with different initial water contents: (a) w_0=205.3%, (b) w_0=258.8%; (c) w_0=305.2%; (d) w_0=487%

Fig. 15 Fitting compression curves of different kinds of clays measured from Xu et al. (2015): (a) Wenzhou slurry; (b) Huaian slurry I; (c) Huaian slurry II

Fig. 16 Comparison of measured and calculated results of the oedometer tests in this study: (a) Kaolin clay with w_0=205.3% (3.5LL); (b) Kaolin clay with w_0=258.8% (4.5LL); (c) Kaolin clay with w_0=305.2% (5.3LL); (d) Kaolin clay with w_0=487.0% (8.4LL)

Fig. 17 Stress-dependency of C_α for Kaolin clay in the simulation

Fig. 18 Constitutive models related to the calculation for self-weight consolidation: (a) compression model; (b) permeability model

Fig. 19 Comparison of measured and calculated results: (a) surface height of soil; (b) void ratio distribution

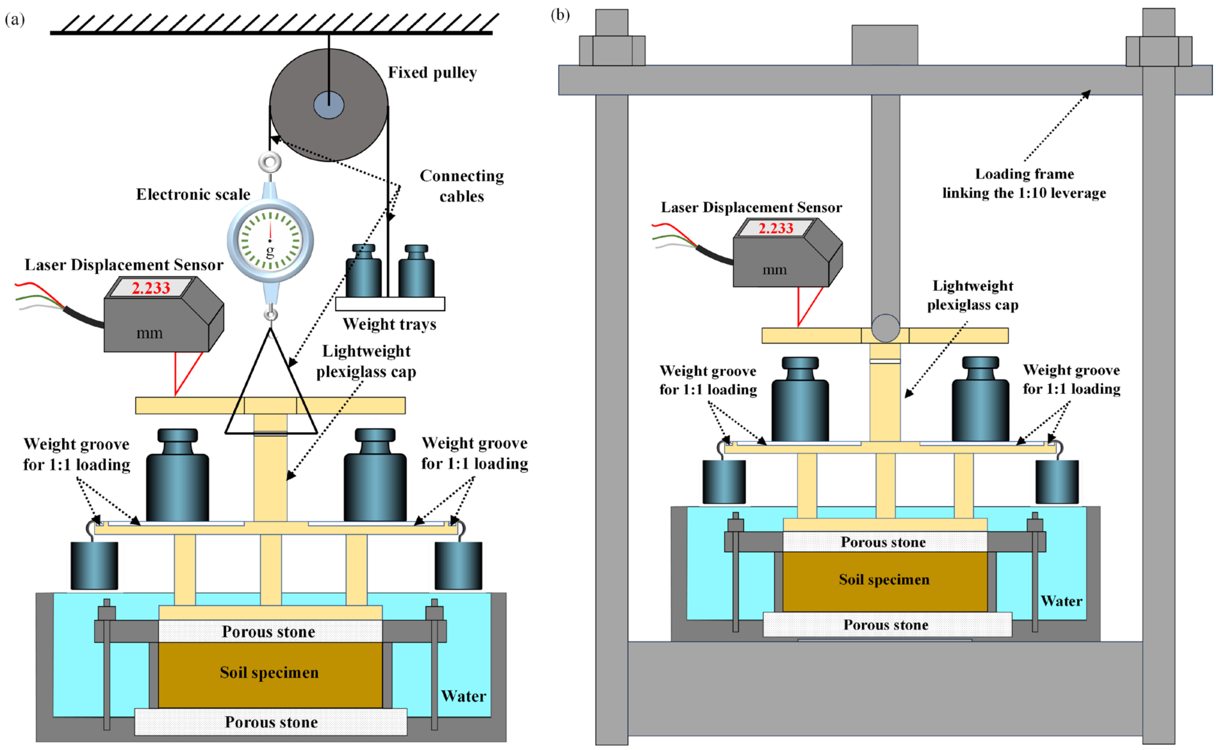

Fig. 1 Modified small stress oedometer system: (a) 1:1 loading stage; (b) 1:10 loading stage

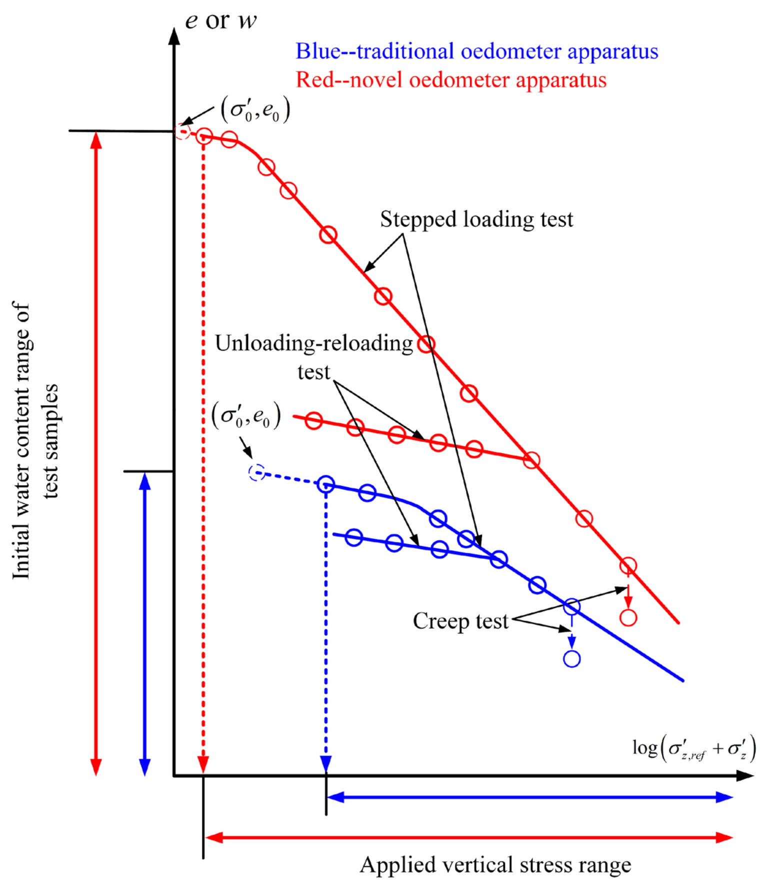

Fig. 2 Schematic diagram of the compression curves obtained using the proposed novel apparatus and a traditional oedometer apparatus

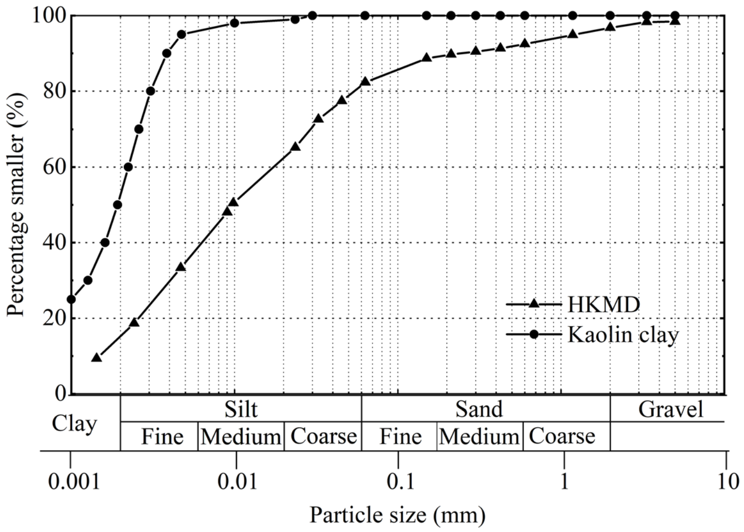

Fig. 3 Particle size distribution curves of test soils

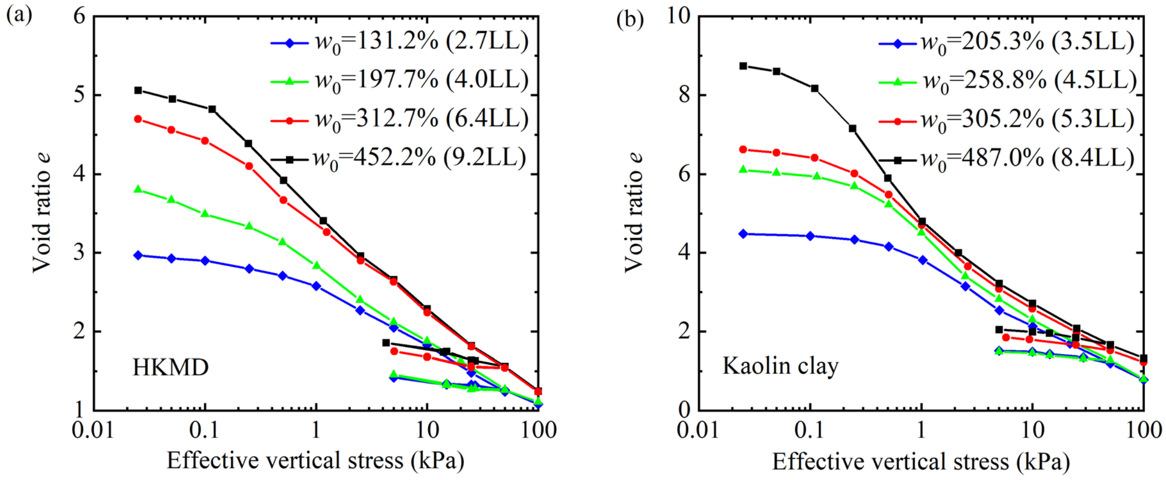

Fig. 4 Compression curves of clays with different initial water contents: (a) HKMD; (b) Kaolin clay

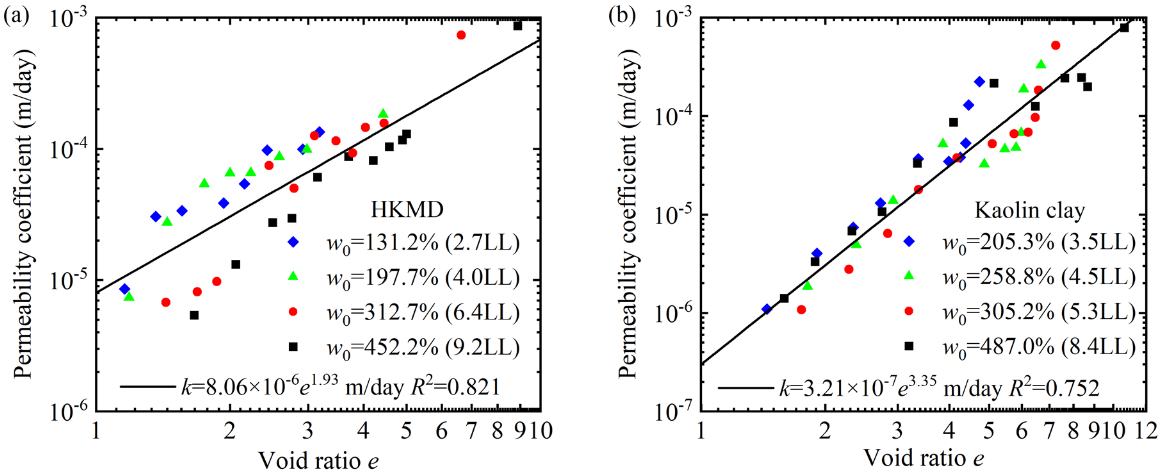

Fig. 5 Relationships between void ratio and permeability coefficient of clays with different initial water contents: (a) HKMD; (b) Kaolin clay

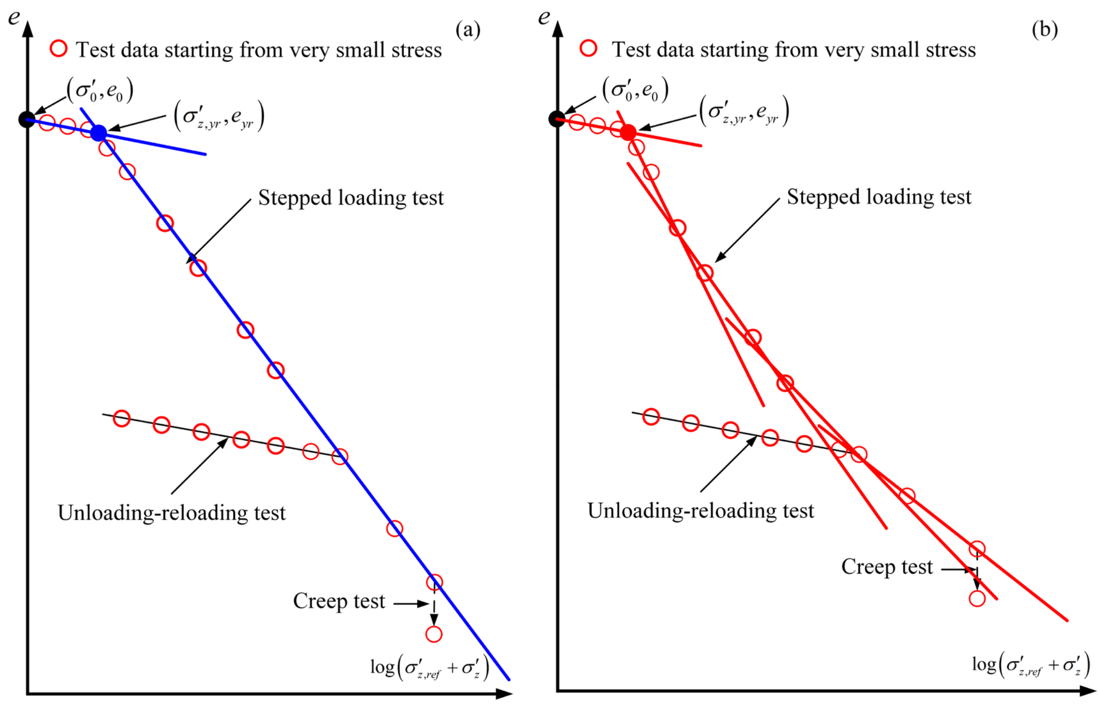

Fig. 6 Schematic diagram of method for determining the remoulded yield stress point: (a) compression curve type with a constant C_c; (b) compression curve type with changing C_c

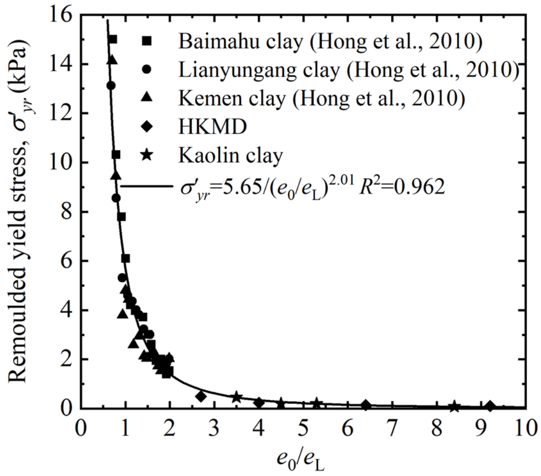

Fig. 7 Relationship between remoulded yield stress and normalized initial void ratio

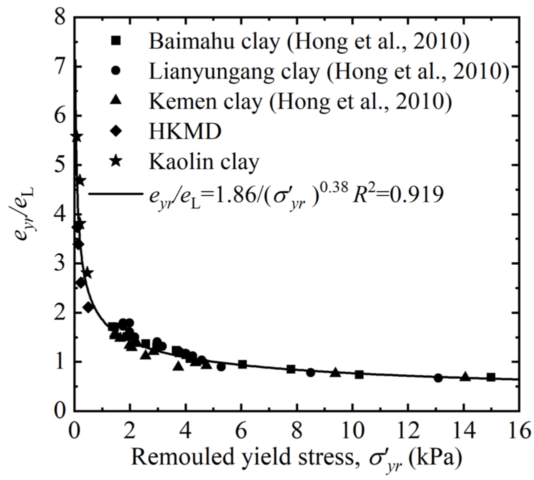

Fig. 8 Relationship between remoulded yield stress and normalized void ratio at remoulded yield stress

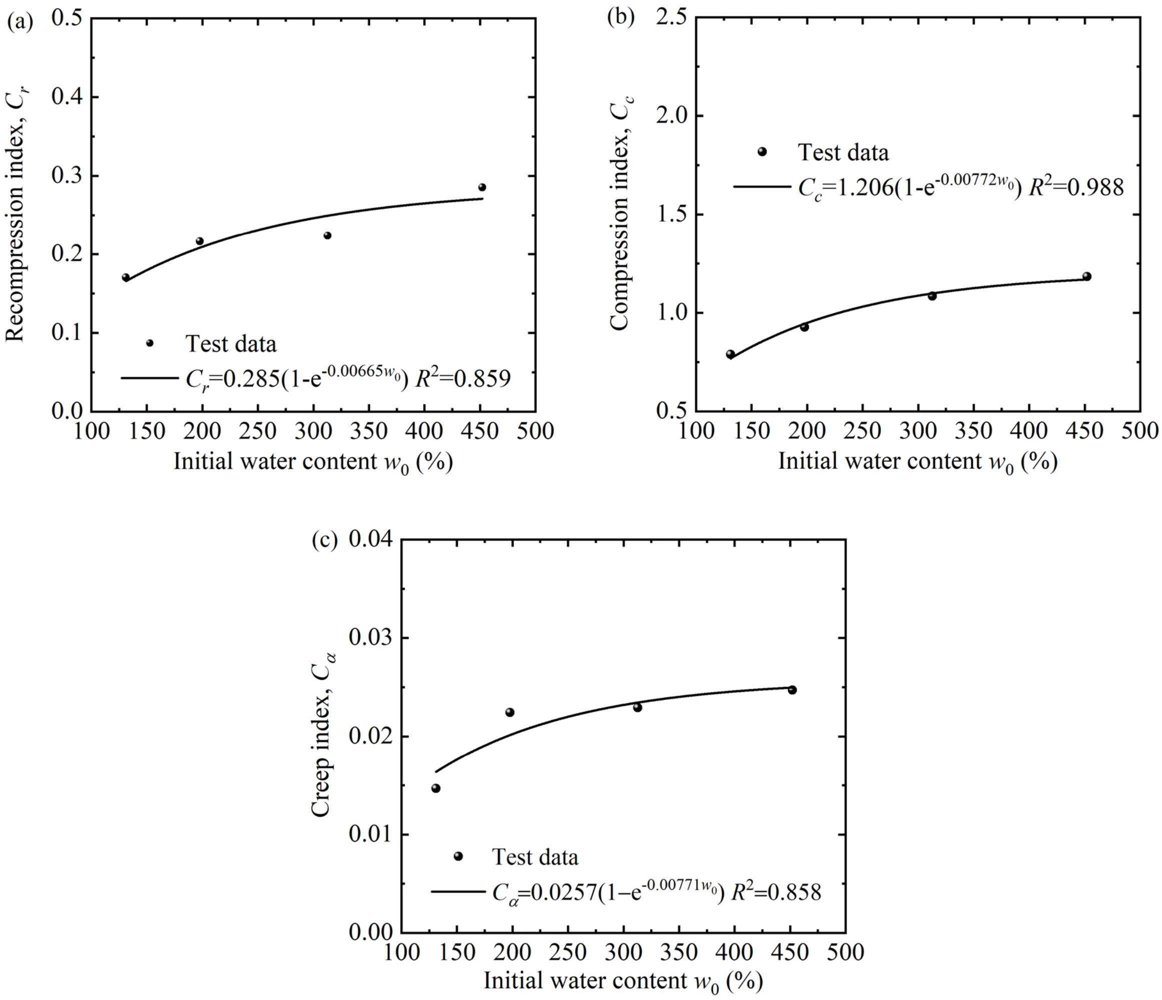

Fig. 9 Compression parameters of HKMD with different initial water contents: (a) C_r; (b) C_c; (c) C_α

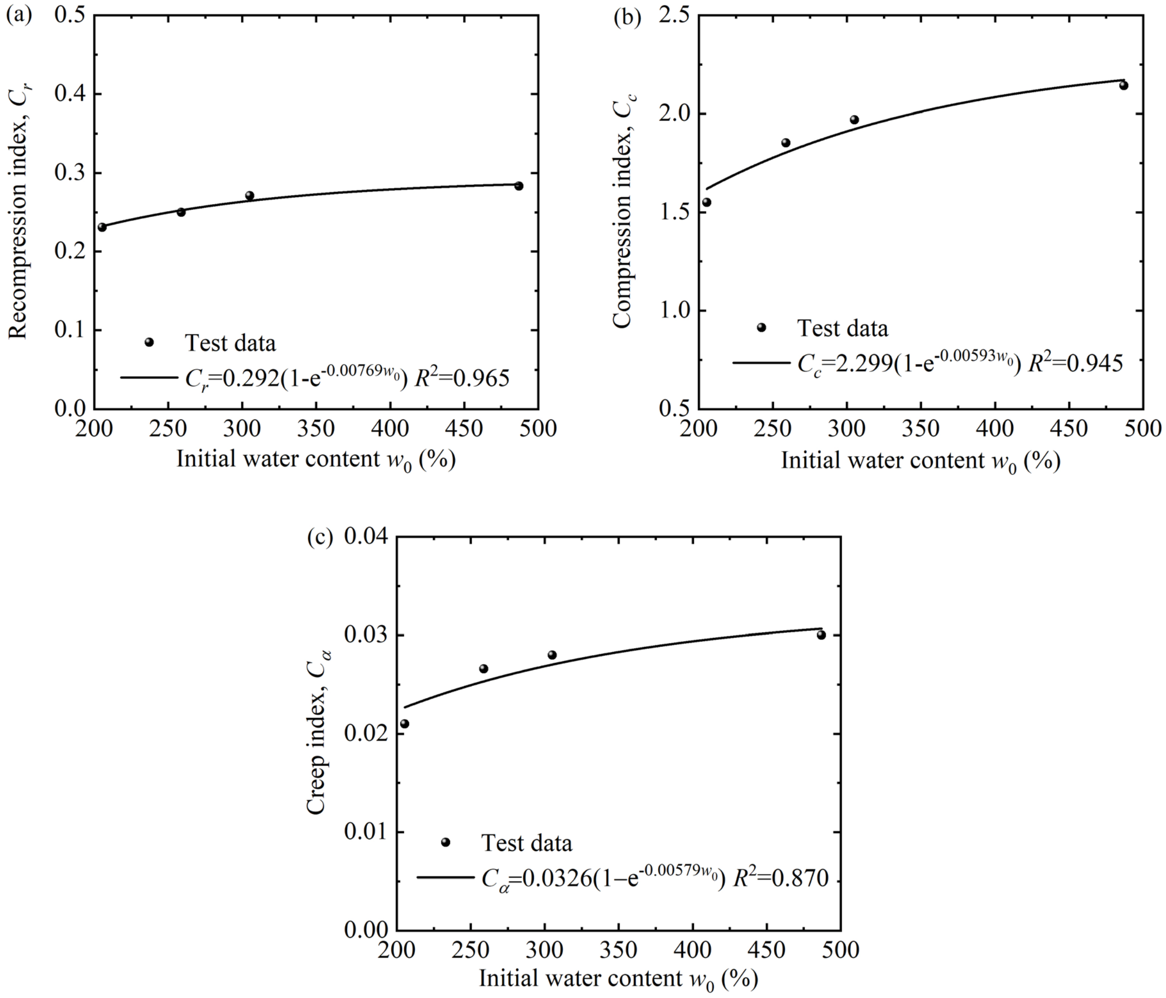

Fig. 10 Compression parameters of Kaolin clay with different initial water contents: (a) C_r; (b) C_c; (c) C_α

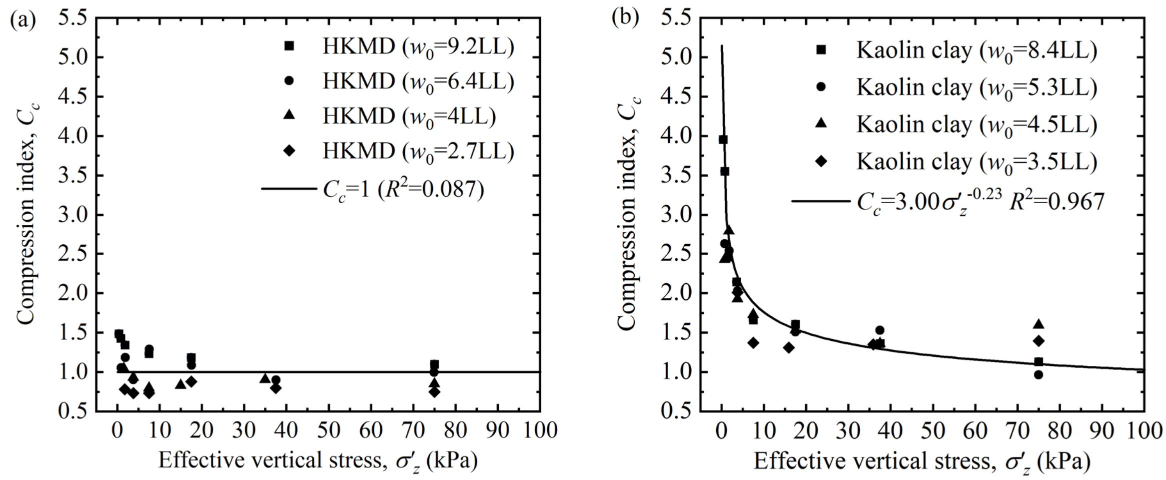

Fig. 11 Compression indexes C_c under different effective stress: (a) HKMD; (b) Kaolin clay

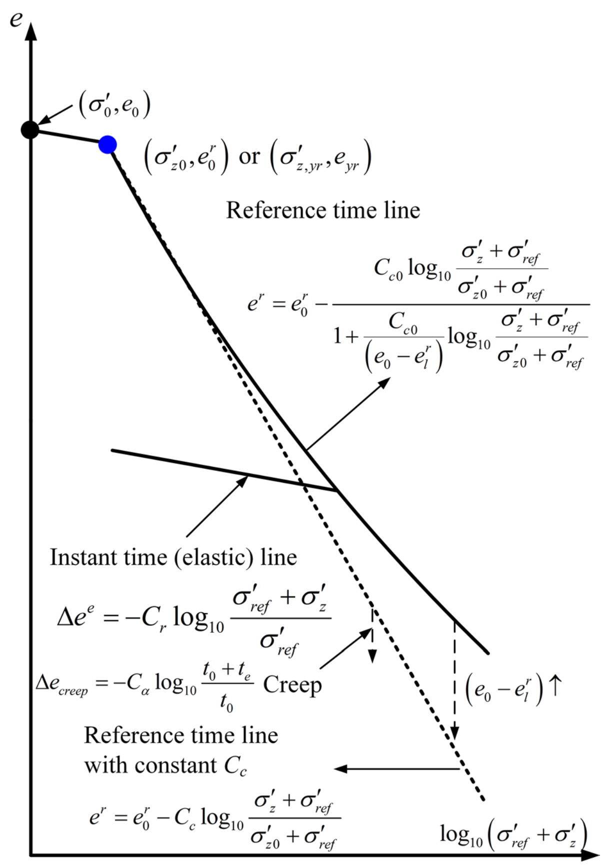

Fig. 12 1D compression relationship with a compression limit for clay with high initial water contents

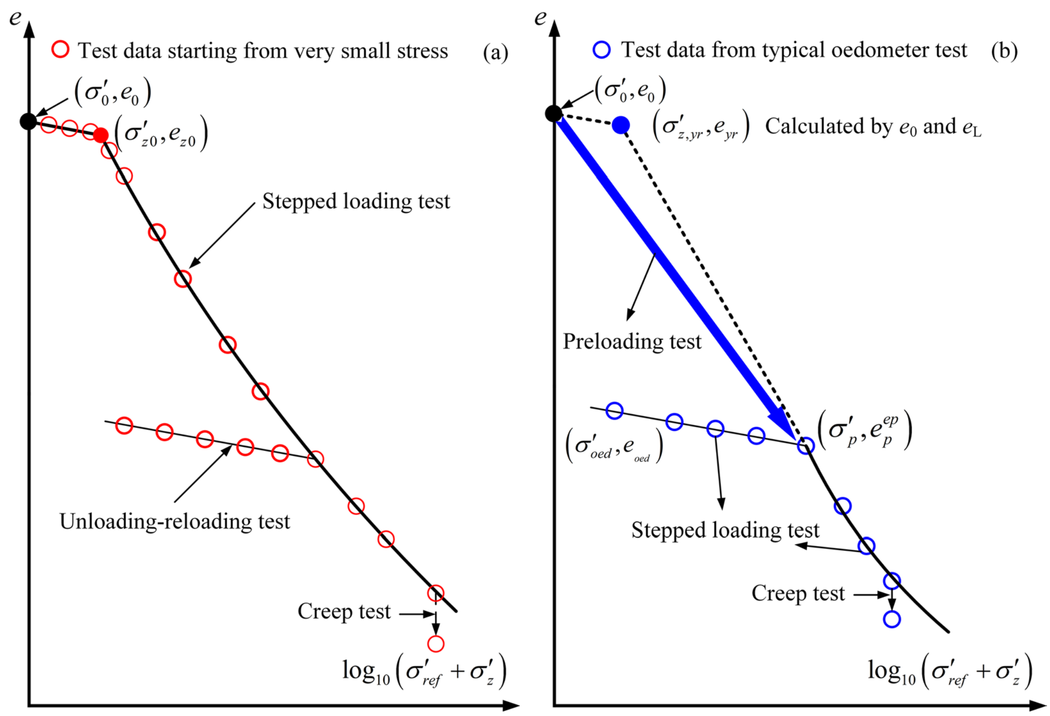

Fig. 13 Methods to obtain the 1D compression relationship of clay with high initial water contents: (a) using enhanced oedometer apparatus; (b) using conventional oedometer apparatus

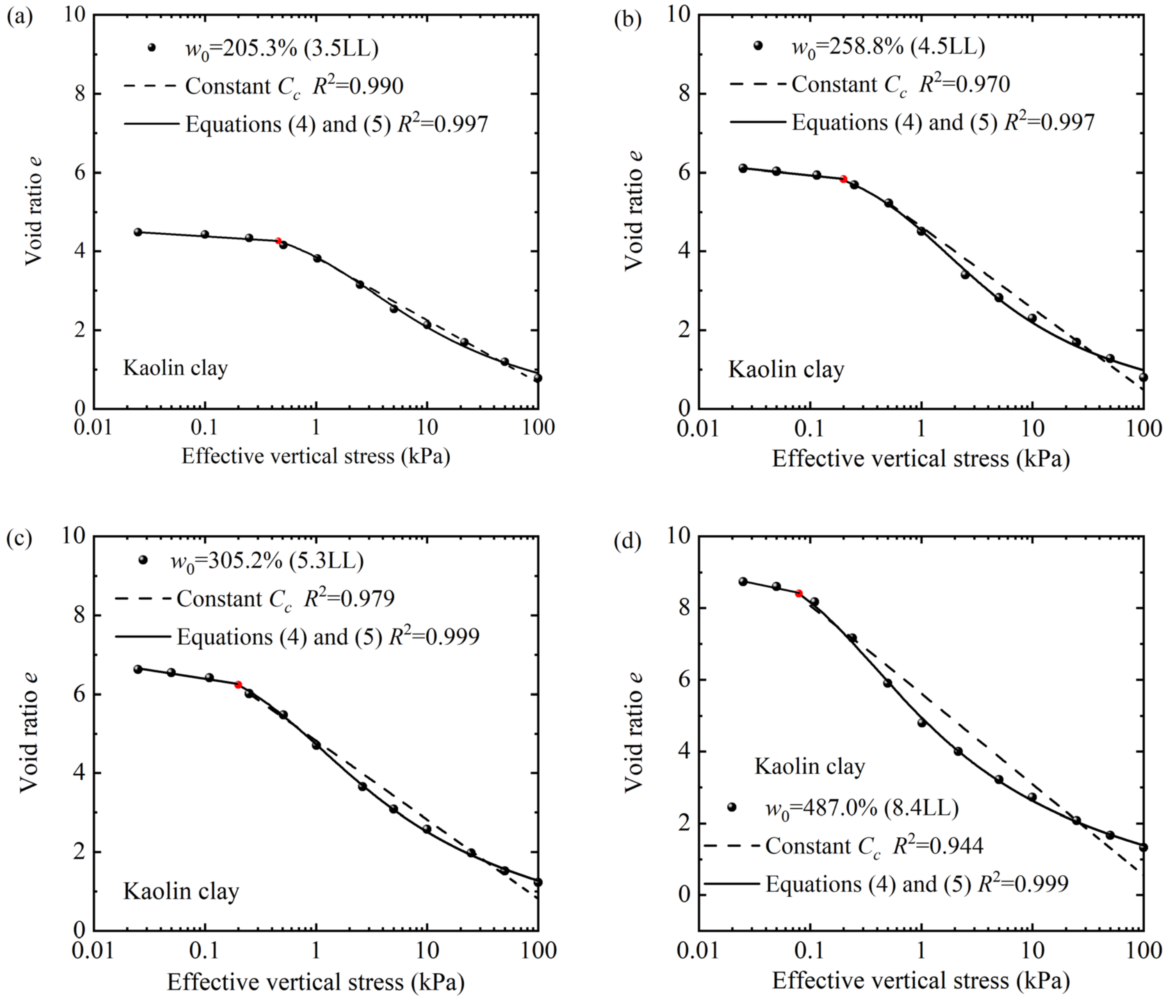

Fig. 14 Fitting compression curves of Kaolin clay with different initial water contents: (a) w_0=205.3%, (b) w_0=258.8%; (c) w_0=305.2%; (d) w_0=487%

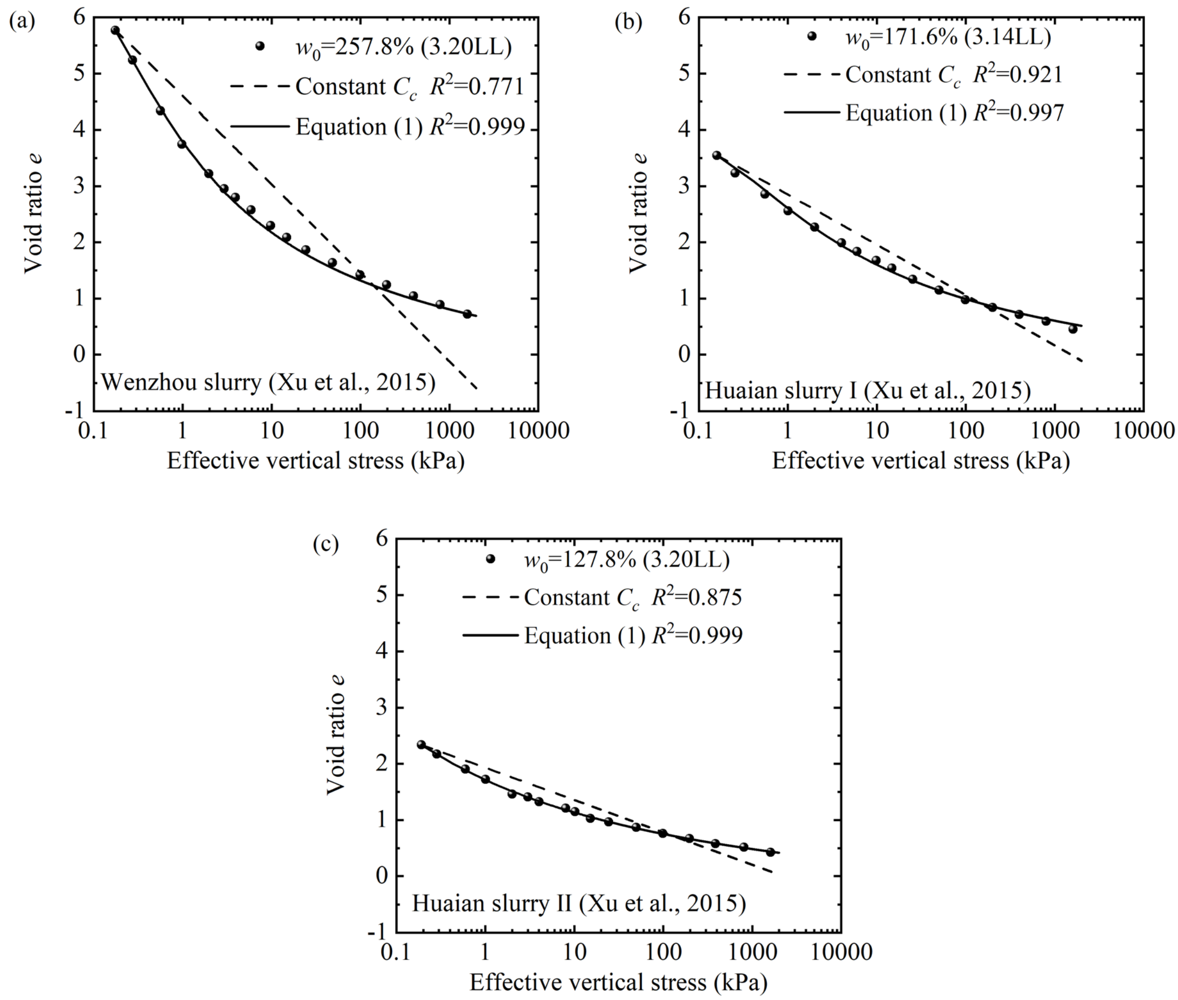

Fig. 15 Fitting compression curves of different kinds of clays measured from Xu et al. (2015): (a) Wenzhou slurry; (b) Huaian slurry I; (c) Huaian slurry II

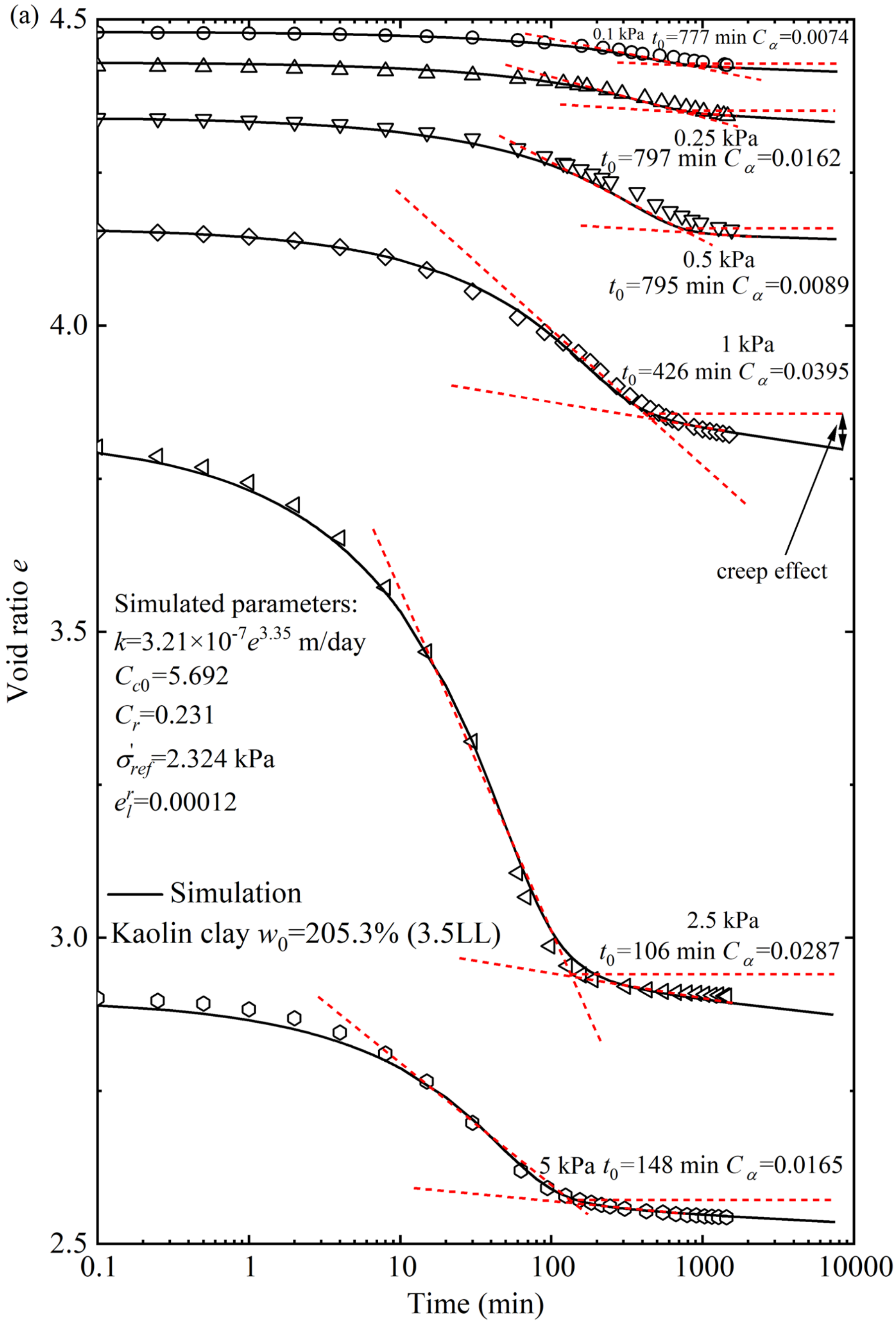

(a)
Void ratio e
Time (min)
0.1 kPa t0=777 min Cα=0.0074
0.25 kPa
t0=797 min Cα=0.0162
0.5 kPa
t0=795 min Cα=0.0089
1 kPa
t0=426 min Cα=0.0395
creep effect
Simulated parameters:
k=3.21×10-7e3.35 m/day
Cc0=5.692
Cr=0.231
σ'ref=2.324 kPa
erl=0.00012
Simulation
Kaolin clay w0=205.3% (3.5LL)
2.5 kPa
t0=106 min Cα=0.0287
5 kPa t0=148 min Cα=0.0165

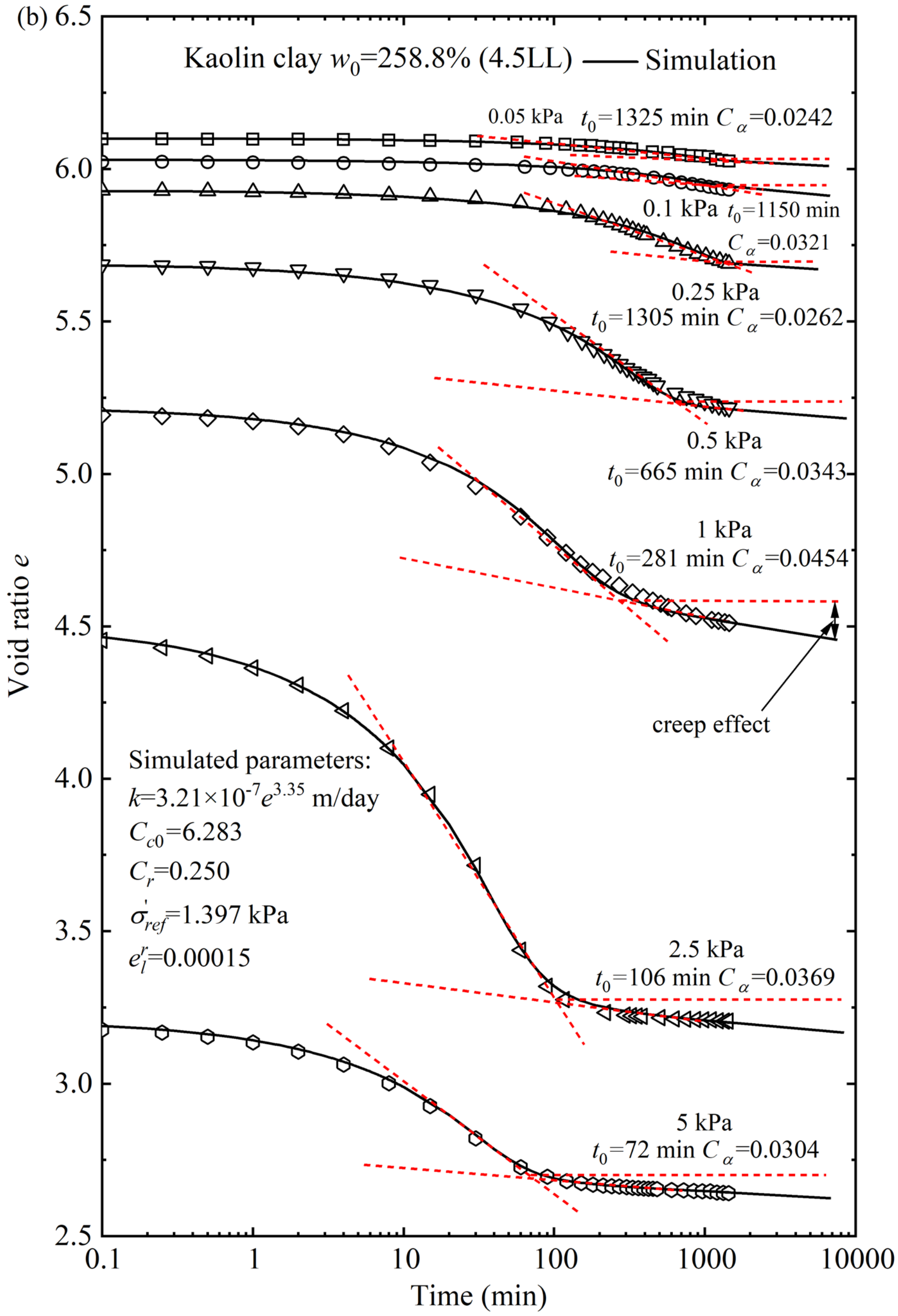

(b)
Kaolin clay w_0=258.8% (4.5LL)
Simulation
0.05 kPa t_0=1325 min C_α=0.0242
0.1 kPa t_0=1150 min C_α=0.0321
0.25 kPa t_0=1305 min C_α=0.0262
0.5 kPa t_0=665 min C_α=0.0343
1 kPa t_0=281 min C_α=0.0454
creep effect
2.5 kPa t_0=106 min C_α=0.0369
5 kPa t_0=72 min C_α=0.0304
Simulated parameters:
k=3.21×10$^{-7}e^{3.35}$ m/day
C_{c0}=6.283
C_r=0.250
σ'_{ref}=1.397 kPa
e_l^r=0.00015
Void ratio e
Time (min)

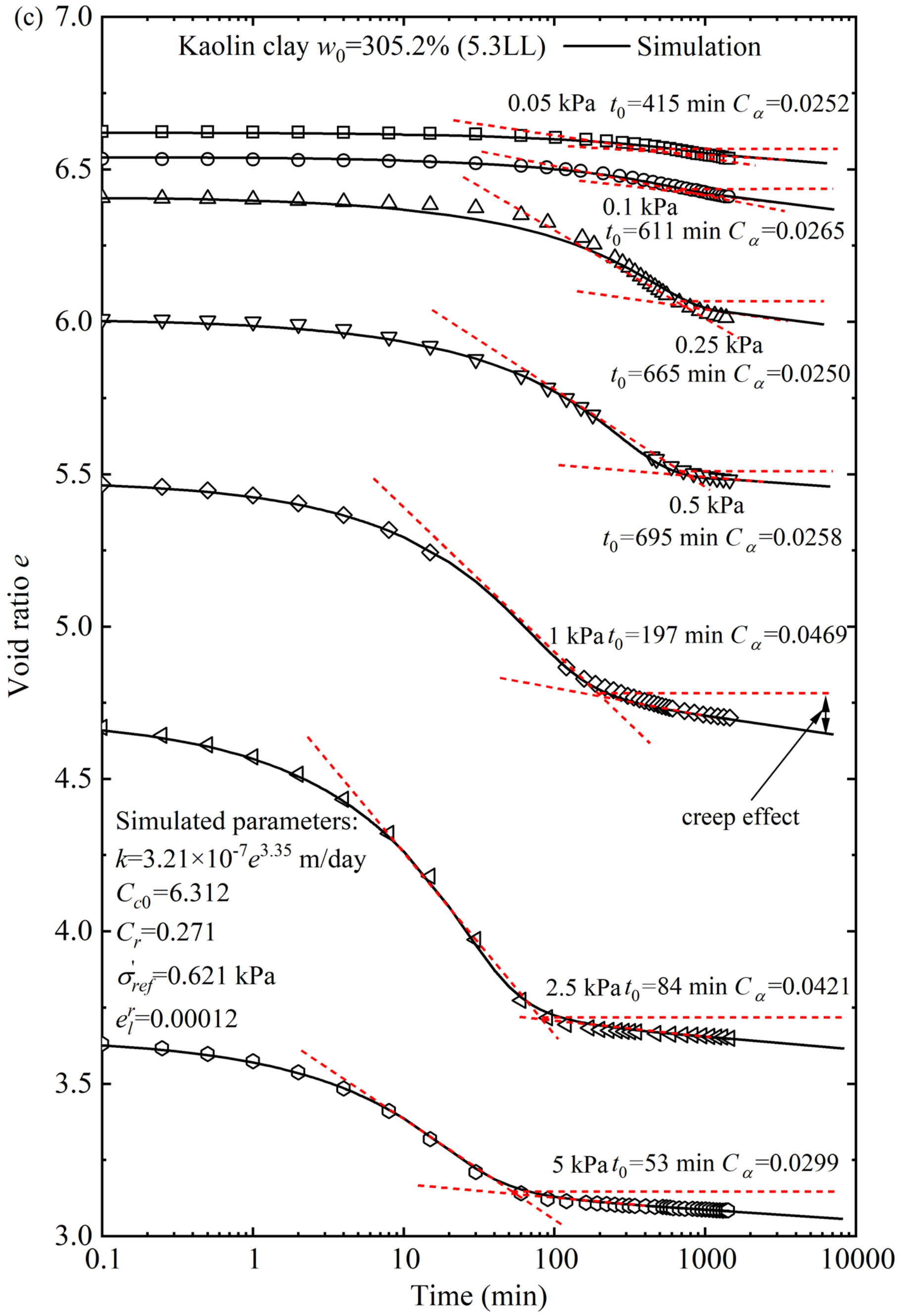

(c)
Kaolin clay w_0=305.2% (5.3LL)
Simulation
0.05 kPa t_0=415 min C_α=0.0252
0.1 kPa
t_0=611 min C_α=0.0265
0.25 kPa
t_0=665 min C_α=0.0250
0.5 kPa
t_0=695 min C_α=0.0258
1 kPa t_0=197 min C_α=0.0469
creep effect
Simulated parameters:
k=3.21×10$^{-7}e^{3.35}$ m/day
C_{c0}=6.312
C_r=0.271
σ'_{ref}=0.621 kPa
e_l^r=0.00012
2.5 kPa t_0=84 min C_α=0.0421
5 kPa t_0=53 min C_α=0.0299
Void ratio e
Time (min)
7.0
6.5
6.0
5.5
5.0
4.5
4.0
3.5
3.0
0.1
1
10
100
1000
10000

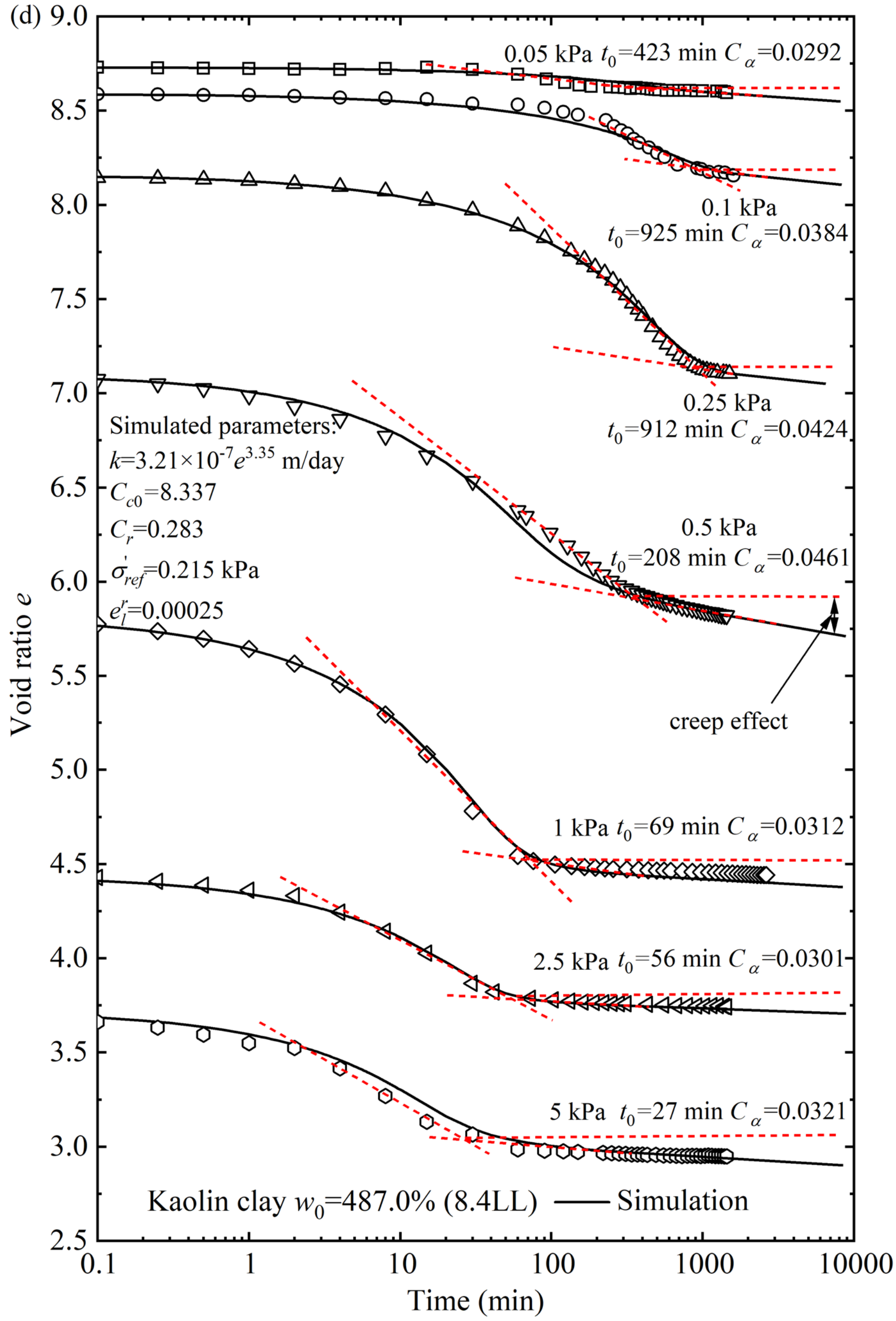

Fig. 16 Comparison of measured and calculated results of the oedometer tests in this study: (a) Kaolin clay with w_0=205.3% (3.5LL); (b) Kaolin clay with w_0=258.8% (4.5LL); (c) Kaolin clay with w_0=305.2% (5.3LL); (d) Kaolin clay with w_0=487.0% (8.4LL)

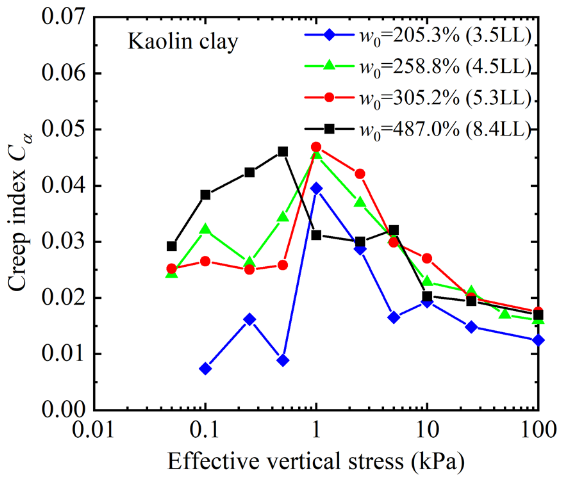

Fig. 17 Stress-dependency of C_α for Kaolin clay in the simulation

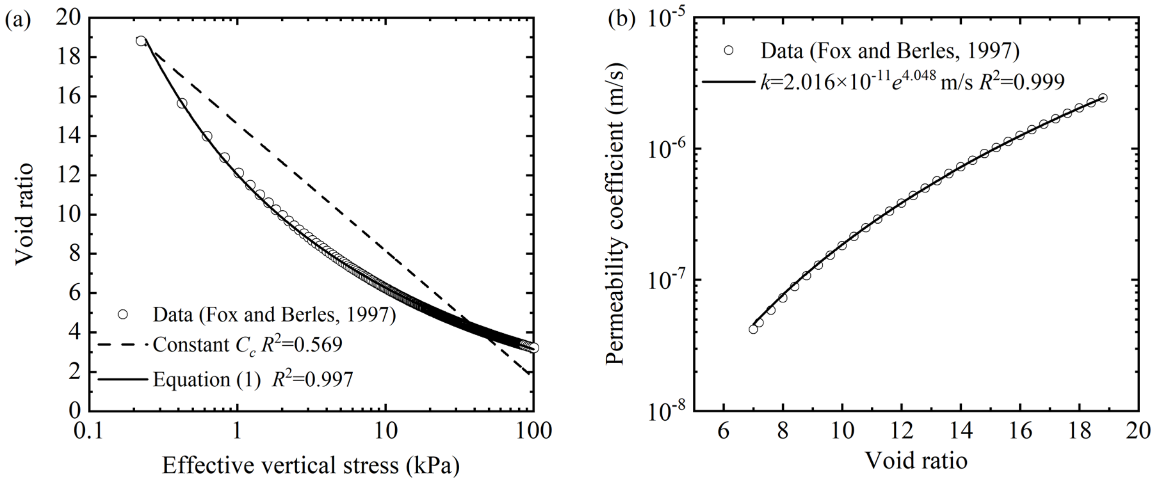

Fig. 18 Constitutive models related to the calculation for self-weight consolidation: (a) compression model; (b) permeability model

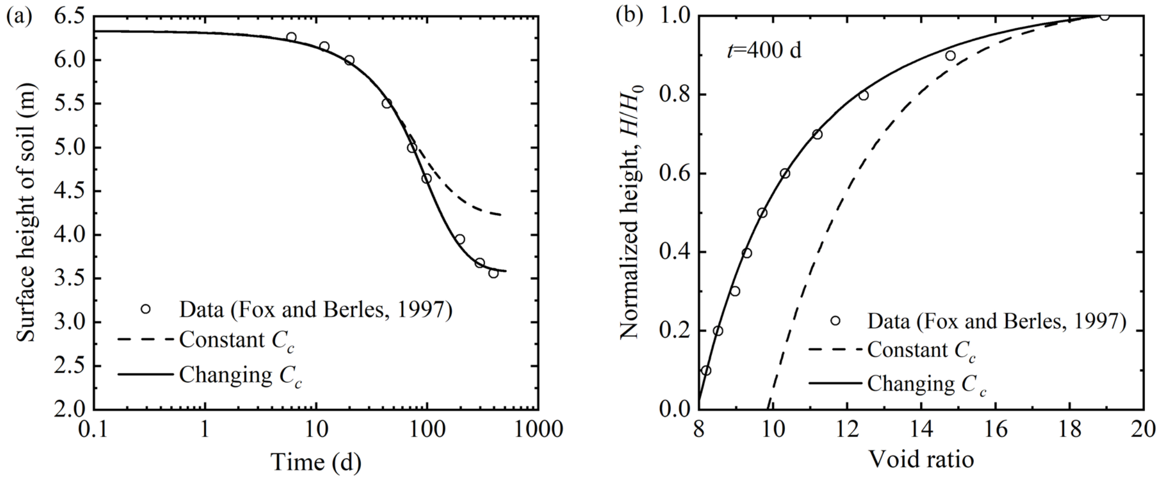

Fig. 19 Comparison of measured and calculated results: (a) surface height of soil; (b) void ratio distribution